Spontaneous Ocular Surface Inflammation and Goblet Cell Disappearance in IκBζ Gene-Disrupted Mice

Mayumi Ueta,[1] *Junji Hamuro,*[1] *Masahiro Yamamoto,*[2] *Kazuhiro Kaseda,*[3] *Shizuo Akira,*[2] *and Shigeru Kinoshita*[1]

Purpose. The ocular surface epithelium is part of the mucosal defense system. Because transcription factor NF-κB in mucosal epithelial cells plays a central role in regulating the genes that govern the onset of mucosal inflammatory responses, we examined the role of a regulator of NF-κB, IκBζ, in murine ocular surface inflammation.

Methods. The eyes of IκBζ$^{-/-}$ mice were analyzed biomicroscopically and histologically. IκBζ expression in normal mouse cornea and conjunctiva was examined by RT-PCR. The results were compared with those obtained in other tissues by real-time PCR. IκBζ mRNA on the ocular surface and in other mucosal tissues was localized by in situ hybridization.

Results. IκBζ$^{-/-}$ mice manifested chronic inflammation, specifically in the ocular surface, but not in other tissues. In normal mice, IκBζ was expressed in a variety of mucosal tissues. The IκBζ transcript was predominantly distributed in the epithelia of these tissues. As inflammatory symptoms progressed on the ocular surface of IκBζ$^{-/-}$ mice, inflammatory cells, mainly CD45R/B220^{+} and CD4^{+} cells, intensely infiltrated the submucosa of the conjunctival epithelia. This infiltration was accompanied by an almost complete loss of goblet cells in the conjunctival epithelia.

Conclusions. The authors postulate that IκBζ in the ocular surface epithelia negatively regulates the pathologic progression of ocular surface inflammation. (*Invest Ophthalmol Vis Sci.* 2005;46:579–588) DOI:10.1167/iovs.04-1055

On the ocular surface, which consists of the conjunctiva and cornea, epithelial cell layers are the initial site of bacterial colonization. Protection of these cell layers against infection from a wide array of pathogens requires robust, innate defense mechanisms.[1–4]

Pathogens must battle nonspecific defense mechanisms, including blinking, tear flow, and mucin, which provide a physical barrier to prevent ocular surface infection under normal conditions.[5,6] In addition to these mechanical defenses, the human tear film contains innate defense molecules with antibacterial properties, such as lysozymes, lactoferrin, and defensins.[4,5] Thus, the ocular surface system presents an inhospitable environment for pathogens seeking to bind to the epithelial cell surface.

However, physiological destruction of the ocular surface by trauma, immunodeficiencies, or routine contact lens wear increases the incidence of sight-threatening corneal infection due to common pathogens, such as *Pseudomonas aeruginosa* and *Staphylococcus aureus*.[7,8] The conjunctival sac and eyelid edge are host to normal bacterial flora including coagulase-negative staphylococci (CNS), *Propionibacterium acnes,* and other commensal Gram-positive and -negative bacteria,[9,10] to which, under normal conditions, the ocular surface epithelia does not respond. Thus, we suggest that there may be a unique inflammation mechanism that prevents corneal opacity or neovascularization.[11]

The mammalian innate immune system plays a key role in recognizing pathogen-associated molecular patterns (PAMPs) through pattern-recognition receptors (PRRs), and in stimulating the production of cytokines and other proinflammatory mediators, followed by the activation of acquired immune responses.[12–17] Members of the Toll-like receptor (TLR) family are essential components in the activation of innate immunity.[5,18–21] If epithelial cells are equipped with a highly sensitive pattern-recognition apparatus, they can be a constant source of proinflammatory mediators.[22]

IκBζ was originally reported as a regulator of transcription factor NF-κB, which is strongly induced by interleukin (IL)-1 and lipopolysaccharide (LPS), but not by tumor necrosis factor (TNF)-α.[23–26] IκBζ, induced by diverse PAMPs such as peptidoglycan (PGN), bacterial lipoprotein, flagellin, MALP-2, R-848, and CpG DNA,[27,28] regulates NF-κB activity, possibly to prevent excessive inflammation caused by bacterial components.[25,27] We used IκBζ gene-disrupted mice to study the role of IκBζ in ocular surface inflammation. These mice expressly exhibited severe, spontaneous ocular surface inflammation, suggesting that IκBζ participates in the negative regulation of ocular surface inflammation.

Materials and Methods

Mice and Reagents

C57BL6 mice were purchased from CLEA (Tokyo, Japan) and used at 8 weeks of age for RT-PCR, semiquantitative RT-PCR, and in situ hybridization of IκBζ. All studies were performed in accordance with the ARVO Statement for the Use of Animals in Ophthalmic and Vision Research.

IκBζ gene-disrupted mice were produced by Shizuo Akira and Masahiro Yamamoto at the Department of Host Defense, Research Institute for Microbial Diseases at Osaka University. To genotype the 2- to 3-week-old mice from heterozygous parents, we used genomic DNA isolated from their tails (DNeasy kit; Qiagen, Valencia, CA). PCR amplification on a thermal cycler (GeneAmp; Applied Biosystems, Foster

From the [1]Department of Ophthalmology, Kyoto Prefectural University of Medicine, Kyoto, Japan; the [2]Department of Host Defense and the [3]Quarters for Experimentally Infected Animals, Research Institute for Microbial Diseases, Osaka University, Osaka, Japan.

Supported in part by grants-in-aid for scientific research from the Japanese Ministry of Health, Labor and Welfare and the Japanese Ministry of Education, Culture, Sports, Science and Technology; a research grant from Kyoto Foundation for the Promotion of Medical Science; and a grant from the Intramural Research Fund of Kyoto Prefectural University of Medicine.

Submitted for publication September 4, 2004; revised October 28, 2004; accepted November 9, 2004.

Disclosure: **M. Ueta**, None; **J. Hamuro**, None; **M. Yamamoto**, None; **K. Kaseda**, None; **S. Akira**, None; **S. Kinoshita**, None

The publication costs of this article were defrayed in part by page charge payment. This article must therefore be marked "*advertisement*" in accordance with 18 U.S.C. §1734 solely to indicate this fact.

Corresponding author: Mayumi Ueta, Department of Ophthalmology, Kyoto Prefectural University of Medicine, Hirokoji, Kawaramachi, Kamigyoku, Kyoto 602-0841, Japan; mueta@ophth.kpu-m.ac.jp.

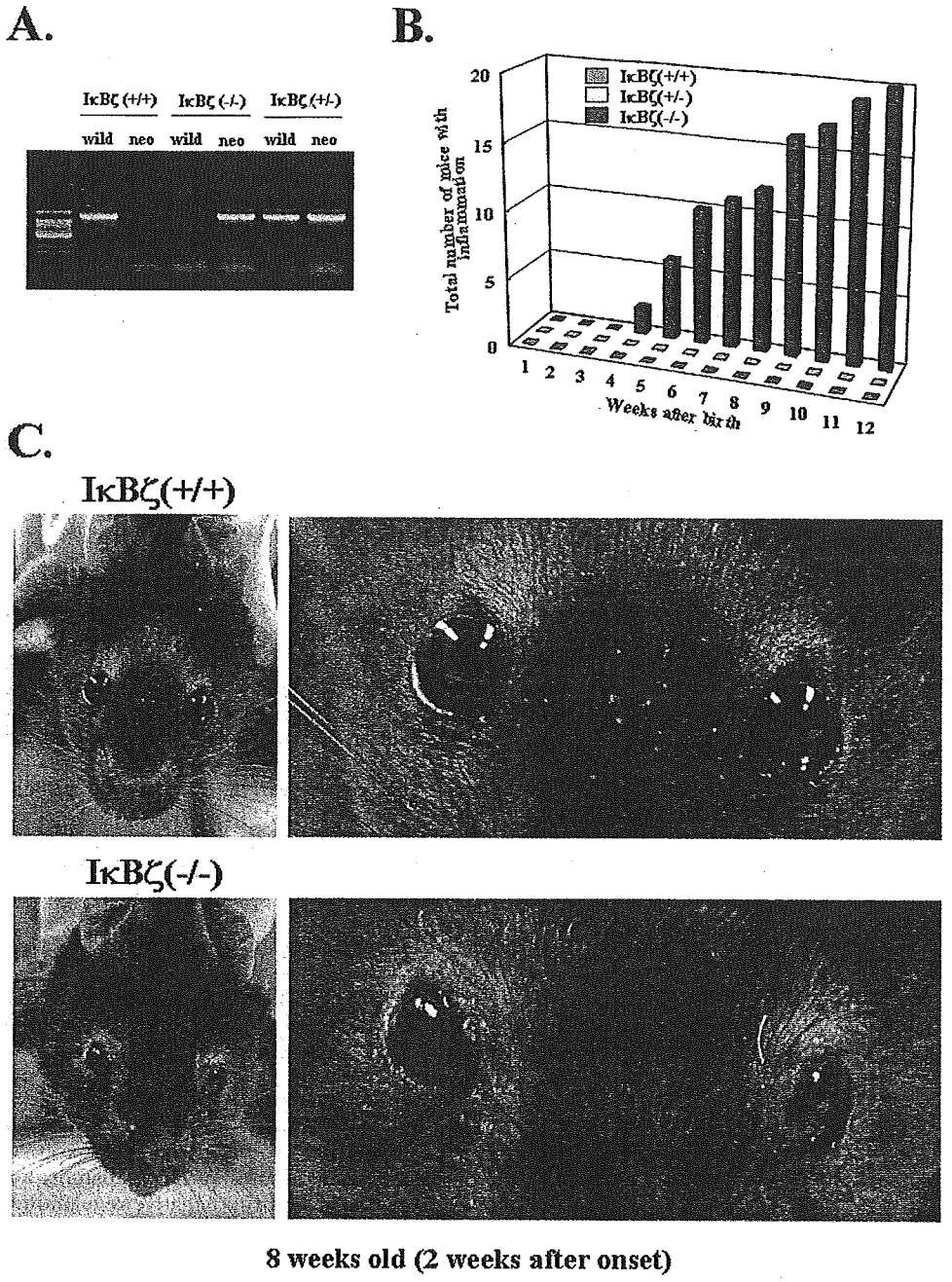

FIGURE 1. Genotype determination of mouse tail genomic DNA and phenotype of IκBζ gene-disrupted mice. (A) PCR products were analyzed on 1% agarose gels. A 1200-bp band was obtained from wild-type mice ($I\kappa B\zeta^{+/+}$) with the IκBζ gene primer pair IκBζ-wild and IκBζ-ex03, another 1200-bp band from homozygotes ($I\kappa B\zeta^{-/-}$) with the gene primer pair IκBζ-ex03 and PKG-rc2, and both fragments from heterozygotes ($I\kappa B\zeta^{+/-}$). (B) The incidence and onset time of ocular surface inflammation in $I\kappa B\zeta^{-/-}$, $I\kappa B\zeta^{+/-}$, and $I\kappa B\zeta^{+/+}$ mice, after birth. Ocular surface inflammation was clinically defined as redness of the eyelid and bulbar conjunctiva, accompanied by discharge. (C) Photographs of the face of a $I\kappa B\zeta^{+/+}$ mouse and an $I\kappa B\zeta^{-/-}$ mouse at 8 weeks of age and at 2 weeks after symptom onset. Whereas $I\kappa B\zeta^{+/+}$ mice were free of inflammation (*top*), $I\kappa B\zeta^{-/-}$ mice exhibited a severe inflammatory phenotype, involving the ocular surface and the eyelids (*bottom*).

City, CA) with the IκBζ gene primer pair for wild IκBζ, IκBζ-wild (GCTCATCCAGCTAACCTGAACAGTGTT) and IκBζ-ex03 (GTTTAAGGTGGCGGTTCTGCTCTTTG), resulted in approximately a 1200-bp fragment from wild-type ($I\kappa B\zeta^{+}/^{+}$) mice. The gene primer pair for the inserted neomycin gene, IκBζ-ex03 and PKG-rc2 (CTAAAGCGCATGCTCCAGACTGCCTTG), yielded approximately a 1200-bp fragment from homozygotes ($I\kappa B\zeta^{-/-}$). Both fragments were obtained from heterozygotes ($I\kappa B\zeta^{+/-}$; Fig. 1A).

LPS was derived from *Escherichia coli* (0111:B4; Sigma-Aldrich, St. Louis, MO).

Histologic Analysis

The whole eyeball, together with the eyelids and conjunctiva, was fixed with 4% paraformaldehyde and embedded in optimal cutting temperature (OCT) compound (Sakura Finetek USA., Inc., Torrance, CA) and then snap frozen in liquid nitrogen. Sections (6 μm thick) were cut and stained with periodic acid-Schiff (PAS) reagent and hematoxylin.

RT-PCR

Using an extraction reagent (TRIzol Reagent; Invitrogen, Carlsbad, CA), we isolated total RNA from mouse tissue and human corneal- and conjunctival epithelial cells according to the manufacturer's instructions. RT was performed (SuperScript Preamplification system; Invitrogen) and then amplification was performed with DNA polymerase (Takara Shiga, Japan) for 30 cycles at 94°C for 1 minute, 60°C for 1 minute, and 72°C for 1 minute (GeneAmp; Applied Biosystems). The primers for mouse IκBζ were (forward), 5′-GAAGCCCGATGAATACCACCCA-3′, and (reverse), 5′-CGCATTGTGAGCCACGACC-3′. For human molecules possessing ankyrin-repeats induced by LPS (MAIL) primers were (forward), 5′-AGGCGATTCAGAAGGAGCAGT-3′ and (reverse), 5′-TCATCAACAGGCGGACAGCAT-3′. For mouse or human

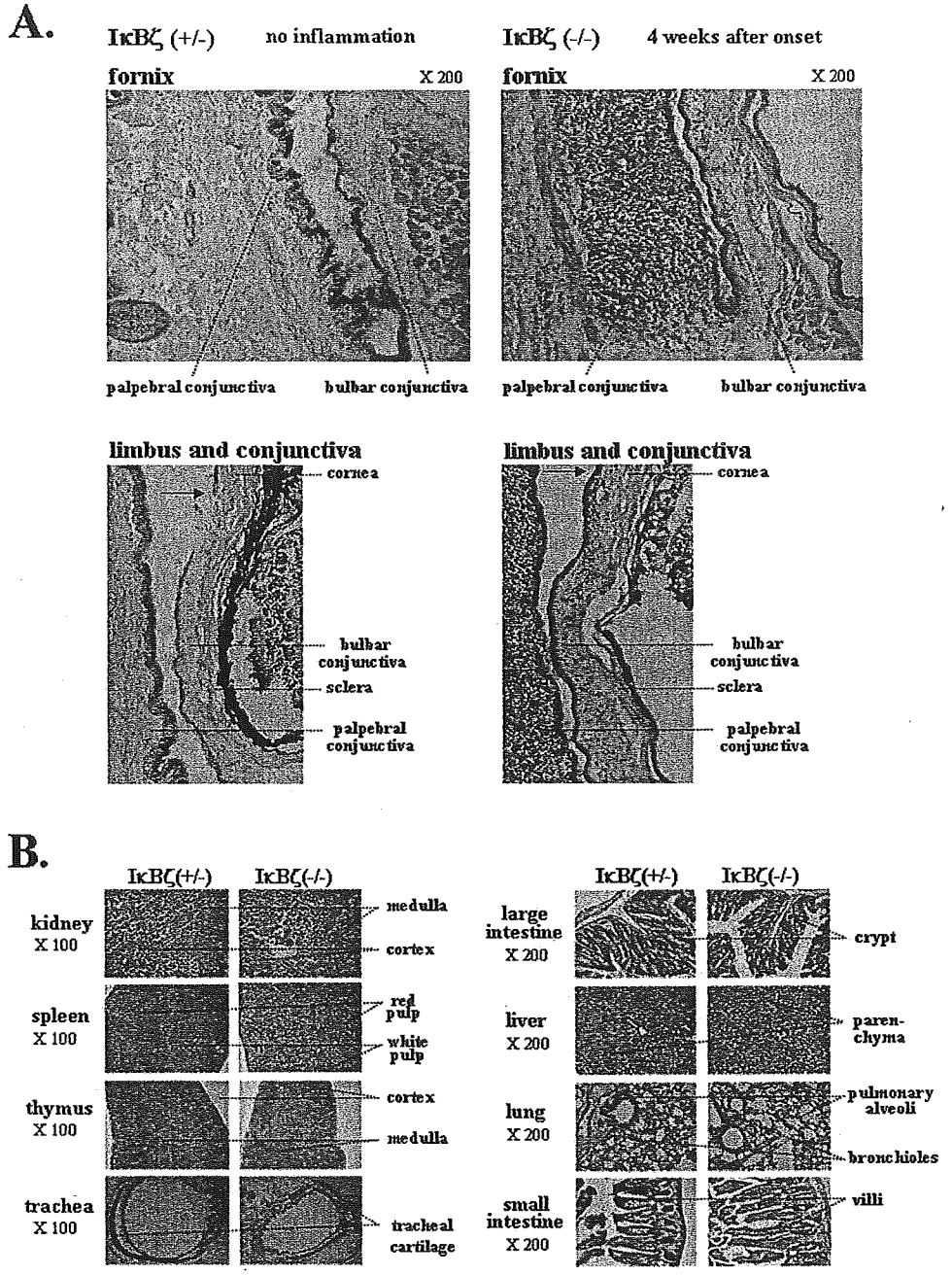

FIGURE 2. Histologic analyses of the eyes of IκBζ$^{-/-}$ mice (PAS stain). (A) Histologic analyses of the eyes of IκBζ$^{-/-}$ mice aged 14 weeks (at 4 weeks after the onset of inflammatory symptoms), revealed heavy infiltration of inflammatory cells into the submucosa under the conjunctival epithelia of the palpebral conjunctiva. There was moderate infiltration in the limbus. In IκBζ$^{-/-}$ mice, there was degeneration and loss of goblet cells in the conjunctival epithelia of both the palpebral and bulbar conjunctiva. The eyes of IκBζ$^{+/-}$ mice of the same age demonstrated neither noticeable pathologic changes nor infiltrating inflammatory cells. *Arrows*: the limbal–corneal junction. (B) In both IκBζ$^{+/-}$ and IκBζ$^{-/-}$ mice, there were no pathologic changes, such as inflammatory phenotypes, in other tissues: kidney, spleen, thymus, trachea, large intestine, liver, lung, and small intestine.

GAPDH they were (forward), 5′-CCATCACCATCTTCCAGGAG-3′, and (reverse), 5′-CCTGCTTCACCACCTTCTTG-3′. The integrity of RNA was electrophoretically confirmed on ethidium bromide–stained 1.5% agarose gels.

Real-Time Semiquantitative PCR

We used a PCR system (Prism 7700; Applied Biosystems), according to the manufacturer's instructions and a previously described protocol.[29] Total cellular RNA extractions and the first cDNA synthesis were as described for RT-PCR. Primer and probes (*Taq*Man; Applied Biosystems) for mouse IκBζ and mouse GAPDH were ready-made assay-on-demand. For IκBζ and mouse GAPDH cDNA amplification, real-time PCR was performed in a 25-μL total volume containing a 1-μL cDNA template in 2× PCR master mix (*Taq*Man Universal PCR Master Mix; Applied Biosystems) at 50°C for 2 minutes and 95°C for 10 minutes, followed by 40 cycles of 95°C for 15 seconds and 60°C for 1 minute. The results were analyzed on computer (Sequence Detection Software; Applied Biosystems), and the level of IκBζ mRNA expression was normalized to the expression of the housekeeping gene GAPDH.

In Situ Hybridization of Mouse Tissues and Human Conjunctiva

Mouse IκBζ cDNA fragments cloned from male mouse kidney cDNA with PCR were used for probes. For PCR cloning, the primers for mouse IκBζ were TGGCCTGACTCCCCTACATT (1663-1682) and CGGGCTGTTCATTCTCCAAG (2078-2059). In situ hybridization was performed as previously described.[30] Briefly, anesthetized C57BL/6 mice were perfusion-fixed with 4% paraformaldehyde, and dissected tissues were sectioned after paraffin embedding.

Human MAIL cDNA fragments cloned with PCR from human kidney cDNA (BD-Clontech, Palo Alto, CA) were used for probes. For PCR cloning, the primers for human MAIL were GCCAACCATTCCAAGTCAGG (854-873) and GCTCCACCTGCCACTGAAAA (1318-1299). Hu-

man conjunctival tissues obtained from patients who had given prior informed consent were fixed with 4% paraformaldehyde and sectioned after paraffin embedding. nitroblue tetrazolium/5-bromo-4-chloro-3-indoyl phosphate (NBT-BCIP) substrate (Roche, Basel, Switzerland) was used to visualize the signal, followed by counterstaining with nuclear fast red. Throughout, the corresponding sense probes did not give rise to staining. The DNA templates used for preparation of the digoxigenin-labeled riboprobes were as described earlier.

Immunohistological Analysis

The whole eyeball, together with the eyelids and conjunctiva, was embedded in OCT compound (Sakura Finetek) and then flash frozen in liquid nitrogen. Sections (6 μm thick) were cut and fixed with 100% acetone at 4°C for 10 minutes and blocked (30 minutes) with 10% normal donkey serum in phosphate-buffered saline (PBS). The primary antibody was applied for 1 hour at room temperature. The rat monoclonal antibody was reactive with mouse CD45R/B220 or mouse CD4 (BD Biosciences, San Diego, CA). The rat IgG2a isotype (BD Biosciences) acted as the negative control. After specimens were washed with PBS, the secondary antibody (Biotin-SP-conjugated AffiniPure $F(ab')_2$ fragment donkey anti-rat IgG(H+L); 1:500 dilution; Jackson ImmunoResearch, West Grove, PA) was applied for 30 minutes. After sections were washed with PBS, they were incubated for 30 minutes (Vectastain ABC Reagent; Vector Laboratories, Inc., Burlingame, CA), washed with PBS, and incubated for 2 minutes with peroxidase substrate solution (3,3'-diaminobenzidine [DAB] substrate kit: Vector), and the slides were then covered with coverslips. Sections were examined under a microscope and photographed with a digital camera.

Human Corneal and Conjunctival Epithelial Cells

For RT-PCR, human corneal epithelial cells were obtained from corneal buttons at the time of corneal transplantation for bullous keratopathy (one eye) and keratoconus (two eyes). Human conjunctival epithelial cells were also obtained by conjunctival brush cytology from three volunteers at the University Hospital of Kyoto Prefectural University of Medicine. The purpose of the research and the experimental protocol were explained to all participants, and their prior informed consent was obtained. All experimental procedures were conducted in accordance with the principles set forth in the Helsinki Declaration.

Results

Ocular Surface of IκBζ Gene-Disrupted Mice

For genotyping of the 2- to 3-week-old mice from heterozygous parents, we used genomic DNA isolated from their tails. PCR amplification was performed with the IκBζ gene primer pair (Fig. 1A). We compared the results obtained in IκBζ gene-disrupted ($I\kappa B\zeta^{-/-}$) mice with those in wild-type ($I\kappa B\zeta^{+/+}$) mice and their heterologous ($I\kappa B\zeta^{+/-}$) littermates. Whereas no $I\kappa B\zeta^{+/+}$ and $I\kappa B\zeta^{+/-}$ mice exhibited symptoms of ocular surface inflammation throughout the experimental period (until they reached the age of 24 weeks), $I\kappa B\zeta^{-/-}$ mice became spontaneously symptomatic by 12 weeks (Fig. 1B). Figure 1C shows the face of an $I\kappa B\zeta^{-/-}$ mouse at 8 weeks of age and at 2 weeks after symptom onset. Although $I\kappa B\zeta^{+/+}$ mice had no inflammation, $I\kappa B\zeta^{-/-}$ mice exhibited a severe inflammatory phenotype on the ocular surface, especially along the eyelids. The inflammatory phenotype was absent at the time of their birth. It became evident when they were between 4 and 12 weeks of age. There were no gender differences with respect to the inflammatory phenotype and the age at symptom onset. In other eye compartments such as the lens, retina, uvea, and sclera, there were no pathologic changes in $I\kappa B\zeta^{-/-}$ mice, and they were not different from $I\kappa B\zeta^{+/+}$ mice (data not shown). No special behavioral abnormalities, including the amount of food and water consumed, were observed in $I\kappa B\zeta^{-/-}$ mice. When these mice were kept under conventional conditions, ocular surface inflammation became more prominent. In some animals, this was accompanied by dermatitis-like skin lesions (data not shown).

Histologic analysis of the eyes of $I\kappa B\zeta^{-/-}$ mice aged 14 weeks (4 weeks after the onset of inflammatory symptoms), showed heavy infiltration by inflammatory cells of the submucosal area of the whole conjunctiva and moderate infiltration of the corneal limbus, the junction of the cornea and conjunctiva. Moreover, we noted degeneration and loss of goblet cells in the conjunctival epithelia of both the palpebral and bulbar conjunctiva. Neither obvious pathologic changes nor infiltrating inflammatory cells were detected in the eyes of $I\kappa B\zeta^{+/-}$ mice of the same age (Fig. 2A). No pathologic changes, such as inflammatory phenotypes, were evident in other tissues such

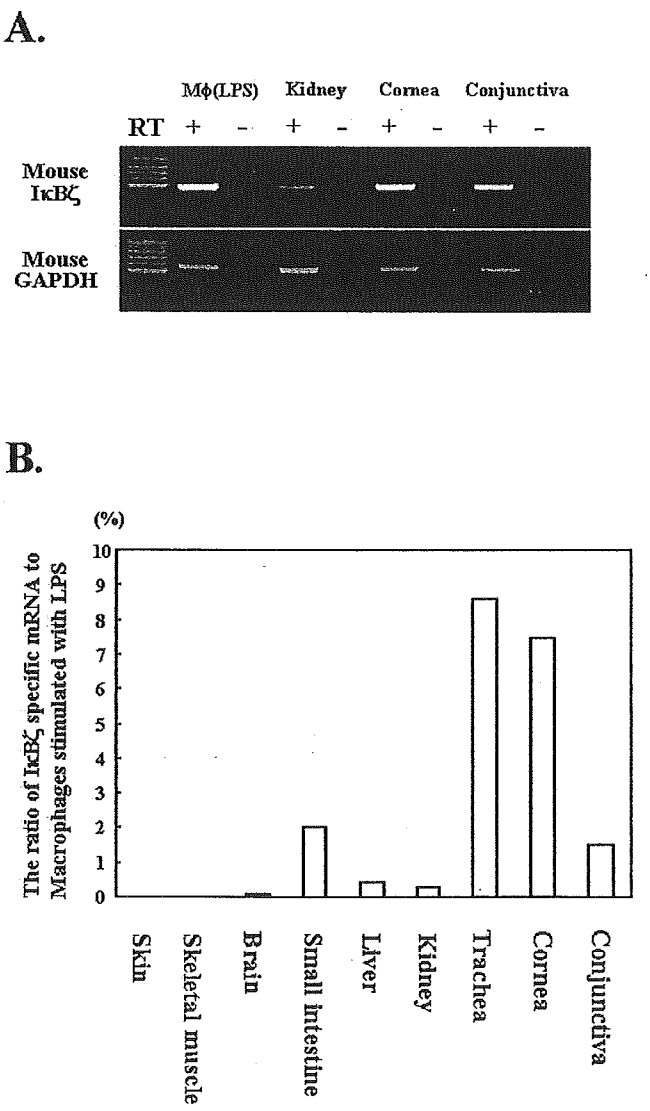

FIGURE 3. Expression of IκBζ mRNA detected by RT-PCR (A) and real-time PCR (B). (A) IκBζ mRNA was expressed in both corneal and conjunctival tissues of normal C57BL/6 mice. We confirmed the specificity of the PCR product for IκBζ by examining peritoneal macrophages stimulated with 100 ng/mL LPS and kidney tissue. (B) IκBζ mRNA was scarcely detected in the skin, skeletal muscle, and brain tissues, slightly expressed in liver and kidney tissues, and intensely expressed in mucosal tissues such as those of the small intestine, trachea, cornea, and conjunctiva.

as those of the kidney, spleen, thymus, trachea, large intestine, liver, lung, and small intestine (Fig. 2B).

IκBζ mRNA Expression

Next, we examined whether ocular surface tissues of mice express IκBζ-specific mRNA. Indeed, IκBζ mRNA was expressed in both corneal and conjunctival tissues of normal C57BL/6 mice (Fig. 3A). We isolated, subcloned, and sequenced the PCR products to ensure the expression of specific IκBζ. The sequences of these PCR products were identical with those of mouse IκBζ. As IκBζ-specific mRNA has been detected in the murine peritoneal macrophages stimulated with LPS, kidney, liver, lung, and heart by Northern blot analysis,[25] we confirmed the specificity of the PCR product for IκBζ by using peritoneal macrophages stimulated with 100 ng/mL LPS and kidney as a positive control.

We then compared the level of IκBζ expression in a variety of murine tissues by using real-time PCR. IκBζ mRNA was scarcely detected in the skin, skeletal muscle, and brain tissue. It was slightly expressed in liver and kidney tissue, and intensely expressed in mucosal tissues, such as the small intestine, trachea, cornea, and conjunctiva (Fig. 3B). Unexpectedly, it was more intensely expressed in the cornea than the conjunctiva, although severe pathologic changes were most evident in conjunctival lesions. This observation suggests interplay between corneal and conjunctival tissues.

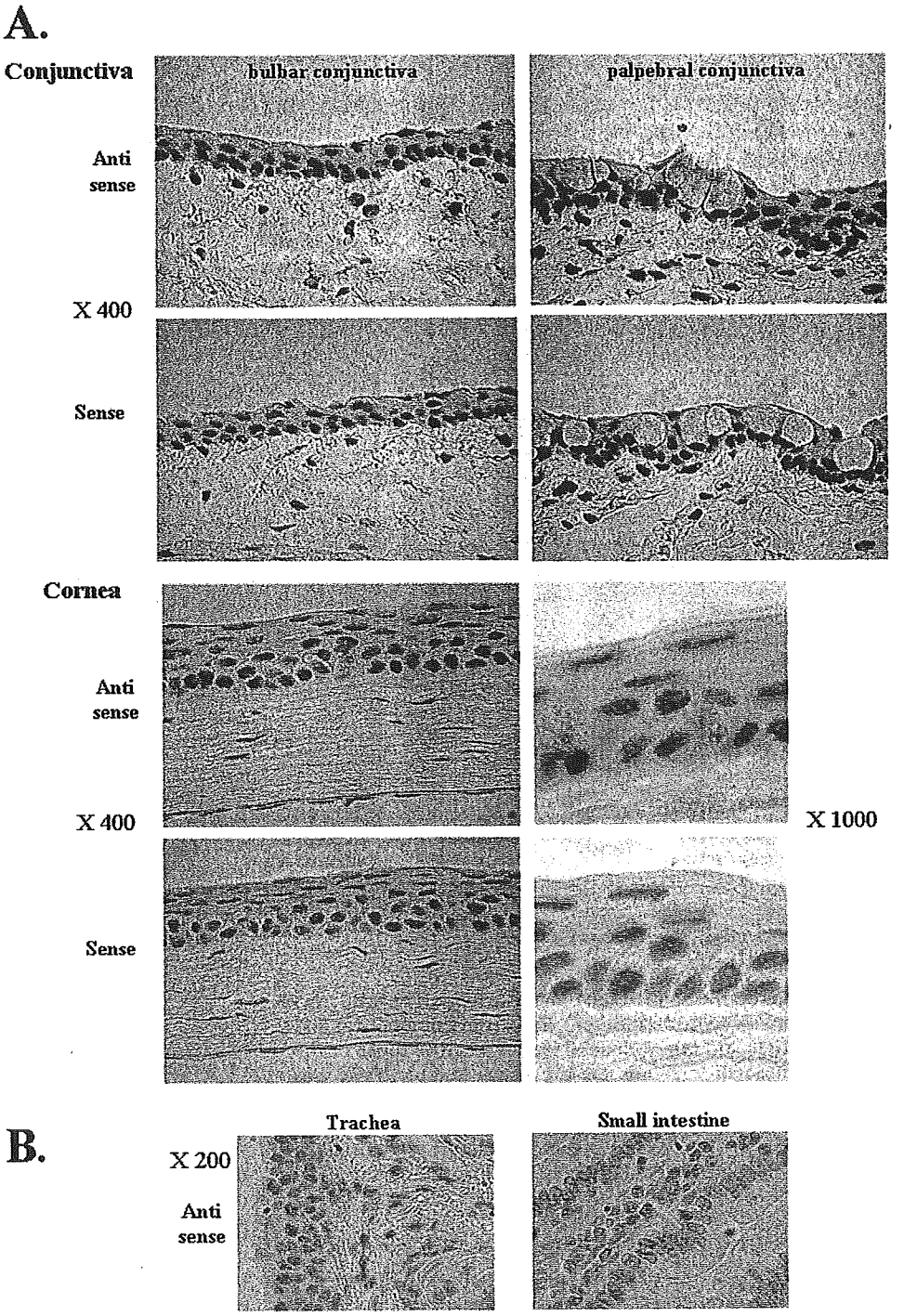

FIGURE 4. In situ hybridization of IκBζ-specific mRNA in ocular surface tissue and other mucosal tissues. The spatial–anatomic distribution of IκBζ transcripts was investigated by in situ hybridization of C57BL/6 conjunctival and corneal tissues and mucosal tissues such as those of the trachea and small intestine. (**A**) IκBζ was expressed in corneal epithelial cells, conjunctival epithelial cells and in some subconjunctival cells. (**B**) The expression of IκBζ transcript was primarily localized in the epithelia of the trachea and small intestine.

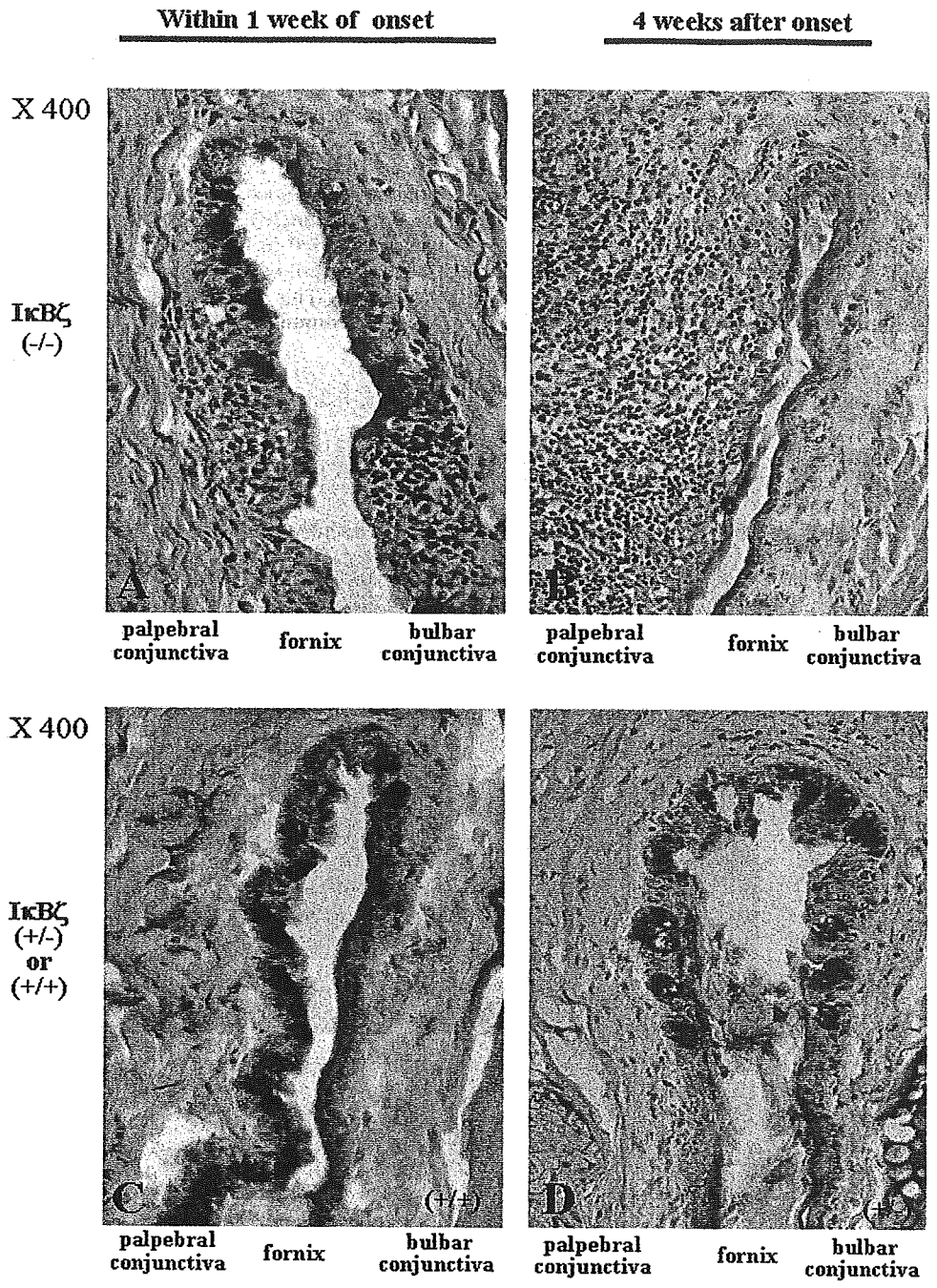

FIGURE 5. Inflammatory infiltrates and loss of goblet cells on the ocular surface of IκBζ$^{-/-}$ mice. Examination of the eyes of 4-week-old IκBζ$^{-/-}$ mice within 1 week after inflammatory symptom onset, showed infiltration of inflammatory cells into the conjunctival epithelia accompanied by simultaneous moderate degeneration of goblet cells (A). The eyes of 14-week-old mice, examined 4 weeks after symptom onset, clearly exhibited the pathologic progression of mucosal inflammation. Note the almost complete loss of goblet cells in the epithelia of both the palpebral and bulbar conjunctiva at this stage (B). In contrast, the eyes of IκBζ$^{+/-}$ or $^{+/+}$ mice did not show any loss of goblet cells or infiltration of inflammatory cells into the conjunctiva (C, D).

Expression of IκBζ in the Ocular Surface Epithelia

We investigated the spatial-anatomic distribution of IκBζ transcript by in situ hybridization of C57BL/6 in conjunctival and corneal tissues and other mucosal tissues, such as those of the trachea and small intestine. On the ocular surface, IκBζ was expressed in corneal epithelial cells, conjunctival epithelial cells, and some subconjunctival cells (Fig. 4A). Furthermore, the predominant expression of IκBζ transcript was localized spatially to the epithelia in the trachea and small intestine (Fig. 4B).

Pathology on the Ocular Surface of IκBζ$^{-/-}$ Mice

We kinetically monitored the pathologic changes in the eyes of IκBζ$^{-/-}$ mice as they grew older. First, we analyzed the eyes of IκBζ$^{-/-}$ mice at 4 weeks of age, within 1 week of the onset of spontaneous inflammatory symptoms. The infiltration of inflammatory cells into the conjunctival epithelia was evident, together with a moderate loss of goblet cells in the conjunctival epithelia (Fig. 5A). The eyes of 14-week-old IκBζ$^{-/-}$ mice (4 weeks after symptom onset), exhibited clear signs of progressive mucosal inflammation. In contrast to the normal spatial distribution of goblet cells in the conjunctival epithelia, which were free from inflammatory infiltrates in IκBζ$^{+/-}$ mice, IκBζ$^{-/-}$ mice manifested heavy infiltration by inflammatory cells under the conjunctival epithelia of the palpebral conjunctiva. There was an almost complete loss of goblet cells in the epithelia of both the palpebral and bulbar conjunctiva in IκBζ$^{-/-}$ mice at this stage (Fig. 5B). Before the manifestation of ocular surface inflammation, the eyes of IκBζ$^{-/-}$ mice exhib-

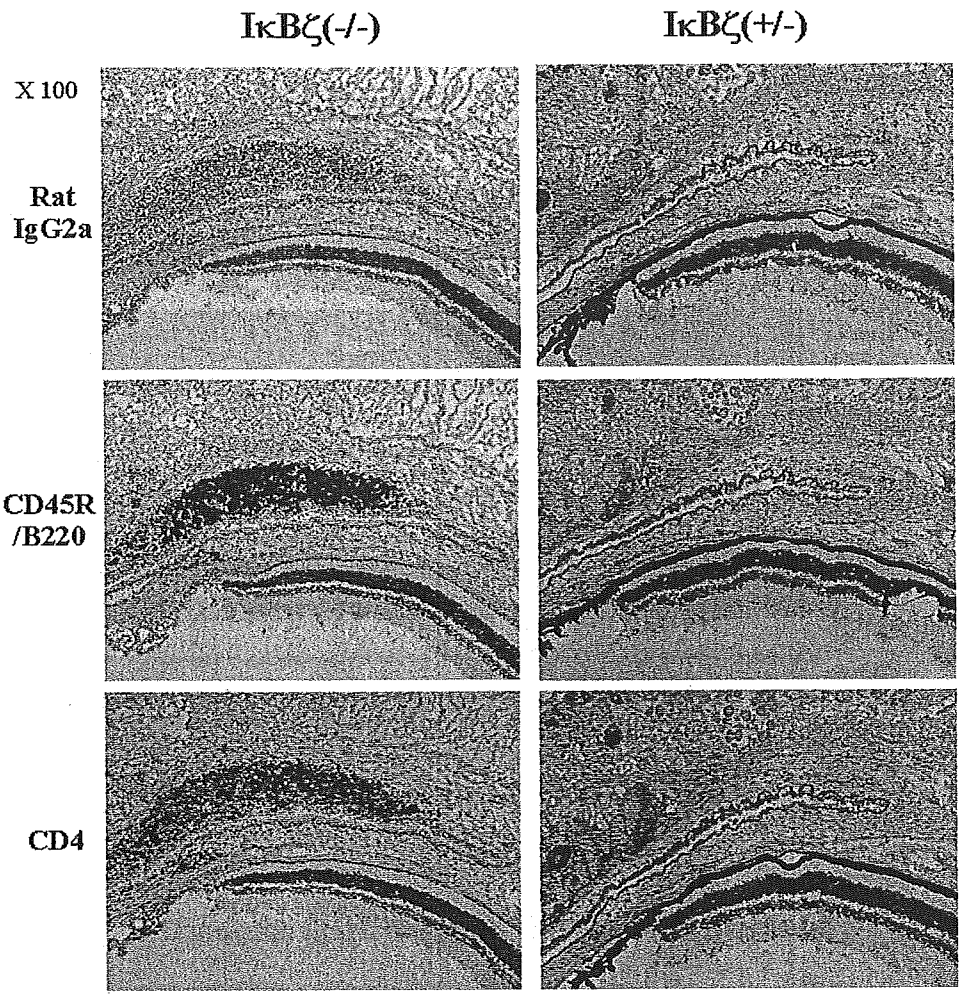

FIGURE 6. Inflammatory infiltrates comprised B- and helper T-cells. Immunohistological analysis of the eyes of IκBζ$^{-/-}$ mice (14 weeks old, 4 weeks after symptom onset) revealed that inflammatory infiltrates in subconjunctival tissues of the eyelid consisted of CD45R/B220^{+} and CD4^{+} cells. Similarly, CD45R/B220^{+} and CD4^{+} cells were detected in the corneal stroma and subconjunctival tissues of the limbus. These cells were not detected immunohistologically in the subconjunctival tissues of IκBζ$^{+/-}$ mice. There was a color difference in the ciliary pigment of epithelial cells. In IκBζ$^{-/-}$ mice the color was brown, and in IκBζ$^{+/-}$ mice it was black.

ited no distinct histologic changes. They were similar to the eyes of IκBζ$^{+/+}$ mice (data not shown). We posit that the observed loss of goblet cells may be a consequence of inflammatory cell infiltration into the conjunctival epithelia of IκBζ$^{-/-}$ mice.

Inflammatory Infiltrates

Using immunohistological analysis, we found that the inflammatory infiltrates in the subconjunctival tissue of the eyelids of 14-week-old IκBζ$^{-/-}$ mice (4 weeks after symptom onset) were CD45R/B220- and CD4-positive cells. These cells were also present in the limbal tissue (Fig. 6). They were not detected in the subconjunctival tissue of IκBζ$^{+/-}$ mice.

Expression of MAIL mRNA on Human Ocular Surface

Human MAIL is reportedly similar to mouse IκBζ.[31] RT-PCR showed that human corneal and conjunctival epithelia expressed MAIL-specific mRNA (Fig. 7A). Isolating, subcloning, and sequencing the PCR products confirmed that they were identical with human MAIL. We further confirmed the specificity of the PCR products for human MAIL with human peripheral monocytes stimulated with 100 ng/mL LPS. In situ hybridization of human conjunctival tissues revealed the restricted spatial distribution of human MAIL transcripts on the ocular surface. Human MAIL was dominantly expressed in conjunctival epithelial cells and moderately expressed in subconjunctival cells (Fig. 7B). Based on these findings, we conclude that a regulator of transcription factor NF-κB, MAIL, is also expressed on the human ocular surface.

DISCUSSION

In IκBζ$^{-/-}$ mice, spontaneous chronic inflammation is selectively elicited in ocular surface tissue but not in other tissues. The IκBζ transcript was predominantly distributed in the epithelia of a variety of mucosal tissues. As the inflammatory symptoms on the ocular surface progressed, inflammatory cells, mainly consisting of CD45R/B220^{+} and CD4^{+} cells, intensely infiltrated the submucosa of the conjunctival epithelia. There was a concurrent loss of goblet cells in the conjunctival epithelia. Our findings suggest that the presence of IκBζ in the ocular surface epithelia inhibits the pathologic progression of ocular surface inflammation. Our observation that a MAIL transcript (a human homologue of mouse IκBζ) was expressed in human corneal and conjunctival epithelia, promotes the new concept that a regulator of NF-κB, MAIL, plays a pivotal role in the pathogenesis of infections via PRRs on the human ocular surface. Studies are under way in our laboratory to determine how IκBζ selectively regulates the pathogenesis of ocular surface inflammation.

The ocular surface is particularly vulnerable to debilitating infections.[4,5,18–21] Although the conjunctival sac and eyelid edge host commensal bacterial flora, under normal conditions there is no inflammatory response by the corneal and conjunctival epithelia. Protection of the eyes from microbial attack is of

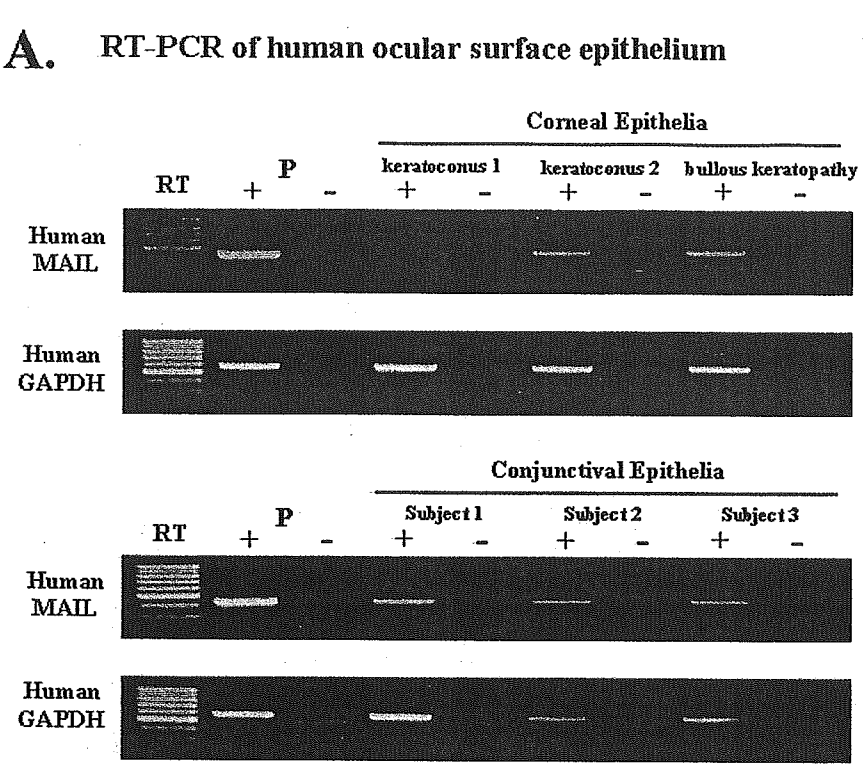

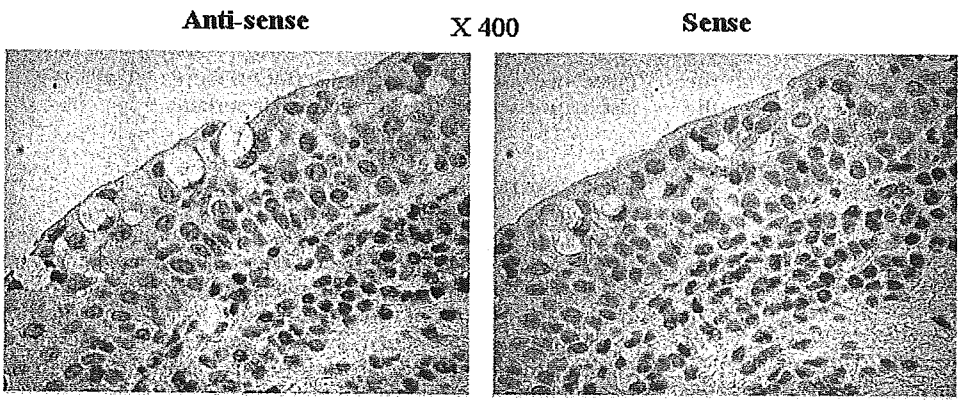

FIGURE 7. Human corneal and conjunctival epithelial tissues expressed MAIL mRNA. (A) RT-PCR detected MAIL-specific mRNA in both the corneal and conjunctival epithelia. The specificity of the PCR product for human MAIL was confirmed by using human peripheral monocytes stimulated with 100 ng/mL LPS. (B) In situ hybridization of human conjunctival tissues revealed the restricted spatial distribution of a human MAIL transcript on the ocular surface. Human MAIL was dominantly expressed in conjunctival epithelial cells and moderately expressed in subconjunctival cells.

paramount importance, as diseases of the ocular surface, in particular corneal infection, can have devastating effects on vision,[4,21] due to the resultant corneal opacity, neovascularization of the cornea, or invasion of the conjunctival epithelia, covering the cornea. Besides possessing several defense modalities in common with other mucosal tissues, the eye has a unique array of protective mechanisms that maintain visual acuity.[1-4]

We have reported[11] that human corneal epithelial cells fail to respond functionally to PAMPs, such as PGN and LPS, due to the lack of TLR2 and TLR4 on their surfaces. Despite the presence of these receptors in the cytoplasm of human corneal epithelial cells, the translocation of LPS to the cytoplasm did not elicit a response by those cells. This suggests that human corneal epithelial cells possess a unique regulatory mechanism to promote the inhibition of TLR2- and TLR4-mediated inflammatory responses. Although the stimulation of macrophages with PGN, LPS, or CpG DNA reportedly results in IκBζ induction,[25,27] we found that stimulation with LPS or CpG DNA did not induce IκBζ in human corneal epithelial cells (data not shown). This suggests that ocular surface epithelial cells possess a unique regulatory mechanism that inhibits TLR-mediated inflammatory responses and contributes to the immunostable environment of the ocular surface epithelia.

To prevent excessive inflammation, the production of pro- and anti-inflammatory mediators must be strictly regulated during the inflammatory course. NF-κB regulates the expression of a wide range of genes,[32-34] including those that encode proinflammatory cytokines and chemokines (e.g., IL-1, IL-6, IL-12,

TNF-α, IL-8, MCP1, RANTES, and eotaxin), adhesion molecules, and inducible effector enzymes (e.g., iNOS and COX-2).[35–37] The production of antimicrobial peptides such as β-defensins, constitutively produced by mucous epithelial cells, is also regulated by NF-κB.[35,36] NF-κB activation also induces the migration and maturation of leukocytes.[37] Furthermore, NF-κB plays a key role in the regulation of apoptosis.[37]

A novel IκB protein, IκBζ/MAIL, induced by IL-1 and PAMPs, but not by TNF-α, regulates NF-κB in the nucleus. The induction of IκBζ is controlled by NF-κB, which, in turn, is regulated by IκBζ. Therefore, NF-κB and IκBζ may comprise an autonomous negative-feedback loop.[27] In contrast, Yamamoto et al.[28] recently reported that IκBζ was indispensable for IL-6 production in response to TLR ligands and IL-1. They proposed a new role for IκBζ as a positive regulator of NF-κB in the two-step process of IL-6 gene activation. IL-6 is a multifunctional cytokine with both pro- and anti-inflammatory effects.[38–41] The former plays an essential role in tissue inflammation and the control of infection. IL-6 can augment or inhibit Th2 tissue inflammation,[42–46] and its anti-inflammatory, counter-regulatory, and healing activities have been documented.[47]

We considered whether the pathologic changes on the ocular surface of IκBζ$^{-/-}$ mice were attributable to an overly robust Th1 or Th2 response due to impaired IL-6 production. However, IL-6$^{-/-}$ mice did not manifest the ocular surface inflammation in IκBζ$^{-/-}$ mice (Akira S, et al., unpublished data, 1995). As IL-6 induces pro- and anti-inflammatory effects that could be tissue or stimulus specific,[48,49] impaired IL-6 production may be the underlying factor in the pathogenesis of ocular surface inflammation in IκBζ$^{-/-}$ mice. Alternatively, the prolonged production of TNF-α in these mice[28] may account for the discrepancies observed in IκBζ$^{-/-}$ and IL-6$^{-/-}$ mice.

Although IκBζ was expressed not only on the ocular surface but also in mucosal tissues such as the trachea and small intestine, in IκBζ$^{-/-}$ mice the inflammatory changes were limited to the ocular surface. The reason for this finding necessitates further investigation. Although regulatory T-cells contribute to the regulation of inflammation in the small intestine,[50] it is not clear whether they play a role in ocular surface inflammation. There is some evidence that the regulation of NF-κB, which dictates inflammatory responses, varies among distinct mucous tissues.[51]

Conjunctival mucosal cells consist of epithelial- and goblet cells that secrete mucin into the tear film. The marked loss of goblet cells in IκBζ$^{-/-}$ mice implies a dramatic decrease of mucin in their tears and a weakening of the innate host defense mechanisms in the ocular surface.[6] Although this weakening may render the ocular surface more highly susceptible to pathogenic and commensal microbes, we currently do not have unequivocal clinical or histologic evidence of bacterial infection in the ocular surfaces of IκBζ$^{-/-}$ mice.

To the best of our knowledge, there have been no rodent models showing the spontaneous loss of goblet cells in their conjunctiva. Rodent models of allergic conjunctivitis displayed no change in these cells,[52–54] and NC/Nga mice with spontaneous atopic dermatitis manifested an increase in goblet cell density.[55] Therefore, IκBζ$^{-/-}$ mice are different from mice with allergy-related conjunctivitis. Considering the regulation of TLRs by NF-κB[12–15] and the induction of IκBζ by TLRs,[25,27] the ocular surface inflammation we observed in the IκBζ$^{-/-}$ mice may be closely related to innate PAMPs/PRRs-amplified immune responses to microbes on the NF-κB axis.

Of particular interest is our observation that IκBζ$^{-/-}$ mice eventually lost almost all goblet cells in the course of persistent inflammation. Humans with devastating ocular surface disorders such as Stevens-Johnson syndrome and ocular cicatricial pemphigoid may experience a similar loss of goblet cells. In a patient with conjunctival inflammation due to Stevens-Johnson syndrome, Kawasaki et al.[56] identified CD4^{+} T-cells in the cell population infiltrating the conjunctival tissues over the cornea. Our findings suggest that IκBζ$^{-/-}$ mice may be a suitable model for Stevens-Johnson syndrome and that these mice may be useful for mimicking the secondary conjunctival inflammation that often occurs in patients with Stevens-Johnson syndrome and/or cicatricial ocular pemphigoid. Moreover, IκBζ$^{-/-}$ mice may provide further insight into the interplay between microorganisms and innate immune responses in the presence of ocular surface disorders.

Acknowledgments

The authors thank Chikako Mochida for technical assistance.

References

1. Philpott DJ, Girardin SE, Sansonetti PJ. Innate immune responses of epithelial cells following infection with bacterial pathogens. *Curr Opin Immunol.* 2001;13:410–416.
2. Williams JM, Fini ME, Cousins SW, Repose JS. Corneal responses to infection. In: Holland EJ, ed. *Cornea.* St. Louis: Mosby; 1997;128–162.
3. Streilein JW. Ocular immune privilege: therapeutic opportunities from an experiment of nature. *Nat Rev Immunol.* 2003;3:879–889.
4. Haynes RJ, Tighe PJ, Dua HS. Antimicrobial defensin peptides of the human ocular surface. *Br J Ophthalmol.* 1999;83:737–741.
5. McClellan KA. Mucosal defense of the outer eye. *Surv Ophthalmol.* 1997;42:233–246.
6. Gipson IK. Distribution of mucins at the ocular surface. *Exp Eye Res.* 2004;78:379–388.
7. Gudmundsson OG, Ormerod LD, Kenyon KR, et al. Factors influencing predilection and outcome in bacterial keratitis. *Cornea.* 1989;8:115–121.
8. Aswad MI, John T, Barza M, Kenyon K, Baum J. Bacterial adherence to extended wear soft contact lenses. *Ophthalmology.* 1990;97:296–302.
9. Doyle A, Beigi B, Early A, et al. Adherence of bacteria to intraocular lenses: a prospective study. *Br J Ophthalmol.* 1995;79:347–349.
10. Hara J, Yasuda F, Higashitsutsumi M. Preoperative disinfection of the conjunctival sac in cataract surgery. *Ophthalmologica.* 1997;211(suppl 1):62–67.
11. Ueta M, Nochi T, Jang MH, et al. Intracellularly expressed TLR2s and TLR4s contribution to an immunosilent environment at the ocular mucosal epithelium. *J Immunol.* 2004;173:3337–3347.
12. Takeda K, Kaisho T, Akira S. Toll-like receptors. *Annu Rev Immunol.* 2003;21:335–376.
13. Akira S, Takeda K, Kaisho T. Toll-like receptors: critical proteins linking innate and acquired immunity. *Nat Immunol.* 2001;2:675–680.
14. Kaisho T, Akira S. Critical roles of Toll-like receptors in host defense. *Crit Rev Immunol.* 2000;20:393–405.
15. Medzhitov R, Janeway CA Jr. Decoding the patterns of self and nonself by the innate immune system. *Science.* 2002;296:298–300.
16. Janeway CA Jr, Medzhitov R. Innate immune recognition. *Annu Rev Immunol.* 2002;20:197–216.
17. Muzio M, Polntarutti N, Bosisio D, Prahladan MK, Mantovani A. Toll like receptor family (TLT) and signalling pathway. *Eur Cytokine Netw.* 2000;11:489–490.
18. Akpek EK, Gottsch JD. Immune defense at the ocular surface. *Eye.* 2003;17:949–956.
19. Pleyer U, Baatz H. Antibacterial protection of the ocular surface. *Ophthalmologica.* 1997;211(suppl 1):2–8.
20. Sack RA, Nunes I, Beaton A, Morris C. Host-defense mechanism of the ocular surfaces. *Biosci Rep.* 2001;21:463–480.
21. Zhang J, Xu K, Ambati B, Yu FS. Toll-like receptor 5-mediated corneal epithelial inflammatory responses to Pseudomonas aeruginosa flagellin. *Invest Ophthalmol Vis Sci.* 2003;44:4247–4254.
22. Platz J, Beisswenger C, Dalpke A, et al. Microbial DNA induces a host defense reaction of human respiratory epithelial cells. *J Immunol.* 2004;173:1219–1223.

23. Kitamura H, Kanehira K, Okita K, Morimatsu M, Saito M. MAIL, a novel nuclear I kappa B protein that potentiates LPS-induced IL-6 production. *FEBS Lett.* 2000;485:53–56.
24. Haruta H, Kato A, Todokoro K. Isolation of a novel interleukin-1-inducible nuclear protein bearing ankyrin-repeat motifs. *J Biol Chem.* 2001;276:12485–12488.
25. Yamazaki S, Muta T, Takeshige K. A novel IkappaB protein, IkappaB-zeta, induced by proinflammatory stimuli, negatively regulates nuclear factor-kappaB in the nuclei. *J Biol Chem.* 2001;276:27657–27662.
26. Muta T, Yamazaki S, Eto A, Motoyama M, Takeshige K. IkappaB-zeta, a new anti-inflammatory nuclear protein induced by lipopolysaccharide, is a negative regulator for nuclear factor-kappaB. *J Endotoxin Res.* 2003;9:187–191.
27. Eto A, Muta T, Yamazaki S, Takeshige K. Essential roles for NF-kappa B and a Toll/IL-1 receptor domain-specific signal(s) in the induction of I kappa B-zeta. *Biochem Biophys Res Commun.* 2003;301:495–501.
28. Yamamoto M, Yamazaki S, Uematsu S, et al. Regulation of Toll/IL-1-receptor-mediated gene expression by the inducible nuclear protein IkappaBzeta. *Nature.* 2004;430:218–222.
29. Tong HH, Chen Y, James M, et al. Expression of cytokine and chemokine genes by human middle ear epithelial cells induced by formalin-killed Haemophilus influenzae or its lipooligosaccharide htrB and rfaD mutants. *Infect Immun.* 2001;69:3678–3684.
30. Takebayashi H, Yoshida S, Sugimori M, et al. Dynamic expression of basic helix-loop-helix Olig family members: implication of Olig2 in neuron and oligodendrocyte differentiation and identification of a new member, Olig3. *Mech Dev.* 2000;99:143–148.
31. Strausberg RL, Feingold EA, Grouse LH, et al. Generation and initial analysis of more than 15,000 full-length human and mouse cDNA sequences. *Proc Natl Acad Sci USA.* 2002;99:16899–16903.
32. Akira S, Kishimoto T. NF-IL6 and NF-kappa B in cytokine gene regulation. *Adv Immunol.* 1997;65:1–46.
33. Ritchie MH, Fillmore RA, Lausch RN, Oakes JE. A role for NF-kappa B binding motifs in the differential induction of chemokine gene expression in human corneal epithelial cells. *Invest Ophthalmol Vis Sci.* 2004;45:2299–2305.
34. McDermott AM, Redfern RL, Zhang B, et al. Defensin expression by the cornea: multiple signalling pathways mediate IL-1beta stimulation of hBD-2 expression by human corneal epithelial cells. *Invest Ophthalmol Vis Sci.* 2003;44:1859–1865.
35. Zhang G, Ghosh S. Toll-like receptor-mediated NF-kappaB activation: a phylogenetically conserved paradigm in innate immunity. *J Clin Invest.* 2001;107:13–19.
36. Ghosh S, May MJ, Kopp EB. NF-kappa B and Rel proteins: evolutionarily conserved mediators of immune responses. *Annu Rev Immunol.* 1998;16:225–260.
37. Karin M, Lin A. NF-kappaB at the crossroads of life and death. *Nat Immunol.* 2002;3:221–227.
38. Kishimoto T. The biology of interleukin-6. *Blood.* 1989;74:1–10.
39. Diehl S, Anguita J, Hoffmeyer A, et al. Inhibition of Th1 differentiation by IL-6 is mediated by SOCS1. *Immunity.* 2000;13:805–815.
40. Jordan M, Otterness IG, Ng R, et al. Neutralization of endogenous IL-6 suppresses induction of IL-1 receptor antagonist. *J Immunol.* 1995;154:4081–4090.
41. Schindler R, Mancilla J, Endres S, et al. Correlations and interactions in the production of interleukin-6 (IL-6), IL-1, and tumor necrosis factor (TNF) in human blood mononuclear cells: IL-6 suppresses IL-1 and TNF. *Blood.* 1990;75:40–47.
42. Anguita J, Rincon M, Samanta S, et al. Borrelia burgdorferi-infected, interleukin-6-deficient mice have decreased Th2 responses and increased lyme arthritis. *J Infect Dis.* 1998;178:1512–1515.
43. Rincon M, Anguita J, Nakamura T, Fikrig E, Flavell RA. Interleukin (IL)-6 directs the differentiation of IL-4-producing CD4+ T cells. *J Exp Med.* 1997;185:461–469.
44. Romani L, Mencacci A, Cenci E, et al. Impaired neutrophil response and CD4+ T helper cell 1 development in interleukin 6-deficient mice infected with Candida albicans. *J Exp Med.* 1996;183:1345–1355.
45. Ohshima S, Saeki Y, Mima T, et al. Interleukin 6 plays a key role in the development of antigen-induced arthritis. *Proc Natl Acad Sci USA.* 1998;95:8222–8226.
46. Ladel CH, Blum C, Dreher A, et al. Lethal tuberculosis in interleukin-6-deficient mutant mice. *Infect Immun.* 1997;65:4843–4849.
47. Dube PH, Handley SA, Lewis J, Miller VL. Protective role of interleukin-6 during Yersinia enterocolitica infection is mediated through the modulation of inflammatory cytokines. *Infect Immun.* 2004;72:3561–3570.
48. Fattori E, Cappelletti M, Costa P, et al. Defective inflammatory response in interleukin 6-deficient mice. *J Exp Med.* 1994;180:1243–1250.
49. Di Santo E, Alonzi T, Poli V, et al. Differential effects of IL-6 on systemic and central production of TNF: a study with IL-6-deficient mice. *Cytokine.* 1997;9:300–306.
50. Groux H, Powrie F. Regulatory T cells and inflammatory bowel disease. *Immunol Today.* 1999;20:442–445.
51. Ghosh S, Karin M. Missing pieces in the NF-kappaB puzzle. *Cell.* 2002;109(suppl):S81–S96.
52. Magone MT, Whitcup SM, Fukushima A, et al. The role of IL-12 in the induction of late-phase cellular infiltration in a murine model of allergic conjunctivitis. *J Allergy Clin Immunol.* 2000;105:299–308.
53. Kunert KS, Keane-Myers AM, Spurr-Michaud S, Tisdale AS, Gipson IK. Alteration in goblet cell numbers and mucin gene expression in a mouse model of allergic conjunctivitis. *Invest Ophthalmol Vis Sci.* 2001;42:2483–2489.
54. Fukushima A, Fukata K, Ozaki A, et al. Exertion of the suppressive effects of IFN-gamma on experimental immune mediated blepharoconjunctivitis in Brown Norway rats during the induction phase but not the effector phase. *Br J Ophthalmol.* 2002;86:1166–1171.
55. Inada N, Shoji J, Tabuchi K, Saito K, Sawa M. Histological study on mast cells in conjunctiva of NC/Nga mice. *Jpn J Ophthalmol.* 2004;48:189–194.
56. Kawasaki S, Nishida K, Sotozono C, Quantock AJ, Kinoshita S. Conjunctival inflammation in the chronic phase of Stevens-Johnson syndrome. *Br J Ophthalmol.* 2000;84:1191–1193.

Characterization and Distribution of Bone Marrow–Derived Cells in Mouse Cornea

Takahiro Nakamura,[1] Fumihiko Ishikawa,[2] Koh-hei Sonoda,[3] Toshio Hisatomi,[3] Hong Qiao,[3] Jun Yamada,[1] Mitsuhiro Fukata,[2] Tatsuro Ishibashi,[3] Mine Harada,[2] and Shigeru Kinoshita[1]

PURPOSE. Bone marrow (BM)–derived stem cells are thought to possess extensive differentiation capacity. The present study was conducted to investigate the characteristics and distribution of these cells in the normal mouse cornea.

METHODS. BM cells and BM-derived hematopoietic stem/progenitor cells (HSCs) from enhanced GFP (eGFP) transgenic mice (lin^-, Sca-1^+) were intravenously transplanted into irradiated wild-type C57BL/6 mice. At 4 to 6 months after transplantation, the mice were killed, and their whole corneas examined by histologic and immunohistochemical methods (CD11c, CD11b, and CD45).

RESULTS. At 2 weeks after BM cell transplantation, GFP^+ cells gradually migrated into the cornea from the limbal area. At 2 to 6 months, they were distributed over the entire cornea. In cross sections of whole cornea, GFP^+ cells comprised 27.3% ± 11.1% (BM) and 24.0% ± 8.01% (HSC) of total cells in the peripheral corneal stroma. In the center of the corneal stroma, GFP^+ cells were 7.58% ± 2.63% (BM) and 8.06% ± 1.76% (HSC) of total cells. Immunohistochemistry showed that GFP^+ $CD11c^+$, $CD11b^+$, $CD11c^-$, and $CD11b^-$ cells occupied the entire corneal stroma.

CONCLUSIONS. The present study provides direct evidence of the distribution of BM-derived cells in the mouse cornea. Immunohistochemical study showed that some of these cells are BM-derived antigen-presenting cells such as dendritic cells and macrophages. Some elements of BM-derived cells may continue to exist in the corneal stroma. (*Invest Ophthalmol Vis Sci.* 2005;46:497–503) DOI:10.1167/iovs.04-1154

Adult somatic stem cells have been isolated from several tissue sources including neurons,[1,2] retina,[3] corneal limbal epithelium,[4,5] and bone marrow (BM).[6–8] It had been thought that somatic stem cells preferentially generate differentiated cells of the same lineage as their tissue of origin. However, recent studies suggest that tissue-specific stem cells can differentiate into lineages other than their tissue of origin and that, with respect to the developmental potential of different adult cell types, there is far more plasticity than previously thought. Particular attention has been focused on the plasticity of BM-derived stem cells. They are reported to possess extensive differentiation capacities and can differentiate into several epithelial types such as liver, lung, and skin.[9] Furthermore, BM-derived mesenchymal stem cells can differentiate in vitro not only into mesenchymal cells, but also into cells with visceral mesoderm, neuroectoderm, and endoderm characteristics.[10] These findings suggest that BM-derived stem cells may have the ability to transdifferentiate into a variety of tissues, including those of the eye.

Normal corneal tissue is located in the anterior segment of the eye, and it participates in several major functions. It is the gateway into the eye of visual images and plays a critical role in maintaining corneal transparency and avascularity. It is composed of three layers: the corneal epithelium, stroma, and endothelium. Corneal epithelial stem cells exist in the basal cell layer of the limbal region[4,5] and in the transitional zone between the cornea and conjunctiva. They are supported by the limbal vascular arcade. Little is known about stem cells of the corneal stroma and endothelium, and the origin of these cells is not well understood.

From an immunologic point of view, the normal avascular cornea was thought to be an immune-privileged site without functional antigen-presenting cells (APCs) and largely devoid of BM-derived cells. Therefore, higher success rates would be expected with corneal than other organ transplants. This notion has lost favor since the demonstration of large numbers of resident BM-derived cells of different lineages—for example, macrophages and dendritic cells—in both the epithelium and stroma of the normal cornea.[11–13] Until now, indirect evidence obtained by immunohistochemical studies has shown these cells to be present and important questions, such as the original cell type and the physiological and functional significance of these progenitors, remain unanswered.

We are the first to attempt the characterization and clarification of the distribution of BM-derived cells in the normal mouse cornea. In the current study, we sought to acquire a direct demonstration by transplanting BM cells from enhanced green fluorescence protein (eGFP) transgenic mice using our unique protocol.[14–16] We transplanted GFP-labeled BM cells and hematopoietic stem/progenitor cells (HSCs) into syngeneic C57BL/6 (wild-type) mice and found BM-derived cells distributed in the mouse cornea. We then evaluated the characteristics of these BM-derived cells by immunohistochemical studies.

MATERIALS AND METHODS

Experimental Animals

The mice were treated in accordance with the ARVO Statement for the Use of Animals in Ophthalmic and Vision Research. The experimental

From the [1]Department of Ophthalmology, Kyoto Prefectural University of Medicine, Kyoto, Japan; and the Departments of [2]Medicine and Biosystemic Science and [3]Ophthalmology, Graduate School of Medical Sciences, Kyushu University, Kyushu, Japan.

Supported in part by Grants-in-Aid for Scientific Research from the Japanese Ministry of Health, Labor, and Welfare and the Japanese Ministry of Education, Culture, Sports, Science, and Technology, and research grants from the Kyoto Foundation for the Promotion of Medical Science and the Intramural Research Fund of Kyoto Prefectural University of Medicine.

Submitted for publication September 29, 2004; revised October 26, 2004; accepted November 3, 2004.

Disclosure: **T. Nakamura**, None; **F. Ishikawa**, None; **K.-h. Sonoda**, None; **T. Hisatomi**, None; **H. Qiao**, None; **J. Yamada**, None; **M. Fukata**, None; **T. Ishibashi**, None; **M. Harada**, None; **S. Kinoshita**, None

The publication costs of this article were defrayed in part by page charge payment. This article must therefore be marked "*advertisement*" in accordance with 18 U.S.C. §1734 solely to indicate this fact.

Corresponding author: Takahiro Nakamura, Department of Ophthalmology, Kyoto Prefectural University of Medicine, Kawaramachi Hirokoji, Kamigyo-ku, Kyoto 602-0841, Japan; tnakamur@ophth.kpu-m.ac.jp.

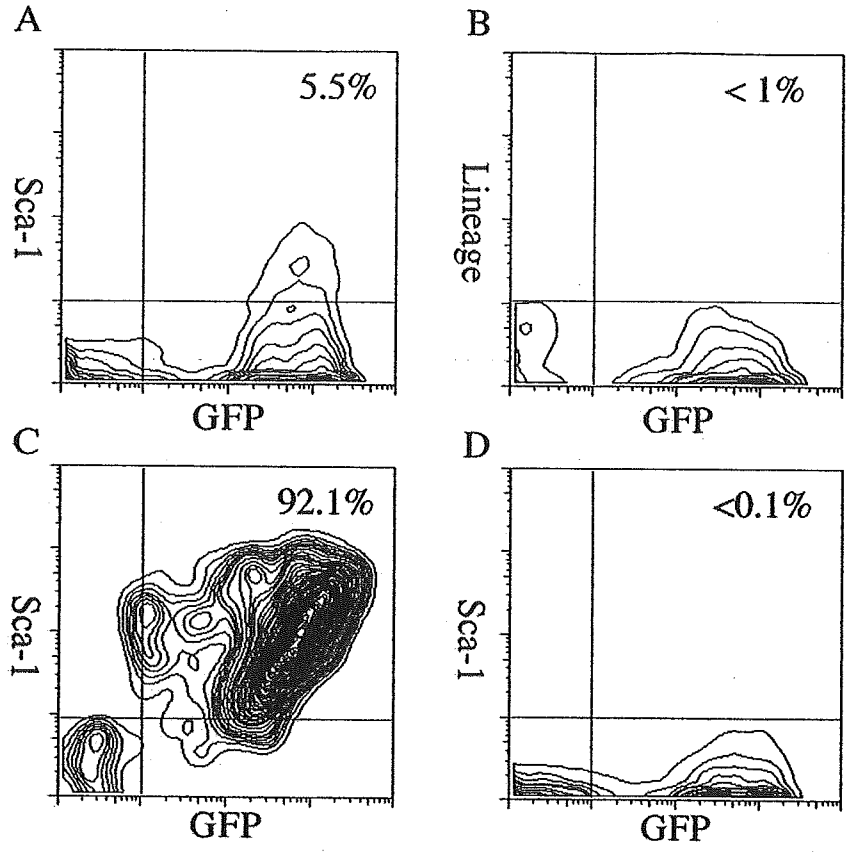

FIGURE 1. Enrichment of hematopoietic stem cells confirmed by flow cytometry. Original BM cells (A). After lineage depletion (B). Positive (C) and negative (D) selection for Sca-1$^+$ cells. After negative and positive selection, the lin$^-$ Sca-1$^+$ cell purity of all GFP$^+$ cells exceeded 95%. Each percentage represents the amount of double-positive cells among all nucleated cells.

procedures were approved by the Committee for Animal Research of Kyoto Prefectural University of Medicine and Kyushu University. Adult (n = 3) and newborn (n = 6) C57BL/6 mice were the recipients of BM cell and HSC transplants, respectively. BM cells were obtained from mice that transgenically express GFP, driven by the chicken β-actin promoter.[17]

Bone Marrow Transplantation

To observe directly the migration of BM-derived cells into the mouse cornea, we used BM cell transplantation.[16] Female eGFP mice (8–10 weeks old) were killed by cervical dislocation while under deep ether anesthesia, and BM cells were obtained by flushing the femurs with sterile phosphate-buffered saline (PBS). The BM cells were washed several times in sterile PBS, filtered twice through a nylon mesh (pore size, 70 μm), counted, and resuspended in PBS at 5×10^7 cells/mL. To generate chimeric mice, all BM cells (6×10^6 to 1×10^7) derived from eGFP transgenic mice were intravenously injected into 8-week-old C57BL/6 recipients that had been lethally x-irradiated with 9 Gy. Their eyes were protected with lead shields to prevent radiation retinopathy. These BM cell transplant recipients were then maintained under special pathogen-free conditions, and successful BM cell transplantation was confirmed by the identification of GFP$^+$ cells in peripheral blood at 2 weeks after transplantation. The corneas of three mice were carefully studied by fluorescence biomicroscopy until 6 months after transplantation. We also used these corneas for histologic and immunohistochemical studies.

Hematopoietic Stem Cell Transplantation

To characterize BM-derived stem/progenitor cells in the mouse cornea, we performed HSC transplantation.[14,15] BM cells were harvested from femurs and tibias of 8- to 12-week-old eGFP mice. Single-cell suspensions of donor cells were prepared by repeated serial passage through a 23-gauge needle. To deplete mature hematopoietic cells, the BM cells were incubated with lineage-specific antibodies (B220, CD3, Gr-1, Mac-1, and TER 119) for 30 minutes at 4°C. After washing with PBS containing 2% fetal bovine serum, the cells were incubated with sheep anti-rat immunomagnetic beads (Dynabeads M-450 coupled to sheep anti-rat IgG; Dynal, Great Neck, NY). Cells not bound to the immunobeads were further purified for Sca-1$^+$ cells. The purity of lineage$^-$ cells was higher than 92% in all experiments. After negative selection of mature hematopoietic and immune cells, positive selection of Sca-1$^+$ cells was performed as just described. After negative and positive selection, the purity of lin$^-$ Sca-1$^+$ cells of all the eGFP$^+$ cells exceeded 95% (Fig. 1).[14,15] To obtain high cell purity, samples were applied twice to columns in each experiment. The resultant 10^4 lin$^-$ Sca-1$^+$ cells were transplanted into C57BL/6 mice within 2 days of their birth. The HSC transplant recipients were maintained under special pathogen-free conditions for 4 weeks. Successful HSC transplantation was confirmed by the identification of GFP$^+$ cells in the peripheral blood at 4 weeks after transplantation. At 4 to 5 months after HSC transplantation, six mice were used for histologic and immunohistochemical studies.

Antibodies

The primary antibodies (all from BD-PharMingen, San Diego, CA) used in this study were purified hamster anti-mouse CD11c (clone HL3), purified rat anti-mouse CD45 (clone 30-F11), and RPE-conjugated rat anti-mouse CD11b (clone M1/70). Secondary antibodies were Cy3-conjugated goat anti-hamster IgG and Cy3-conjugated donkey anti-rat IgG (Vector Laboratories, Inc., Burlingame, CA).

Immunohistochemistry

Immunohistochemical studies of markers for APCs were performed by using a previously reported method[11–13] and a modified version of our method.[18,19] Briefly, freshly excised corneas were fixed for 60 minutes at 4°C in 4% paraformaldehyde, extensively washed with PBS, fast frozen in liquid nitrogen, and embedded in optimal cutting temperature (OCT) compound (Tissue-Tek II; Miles Laboratories, Elkhart, IN).

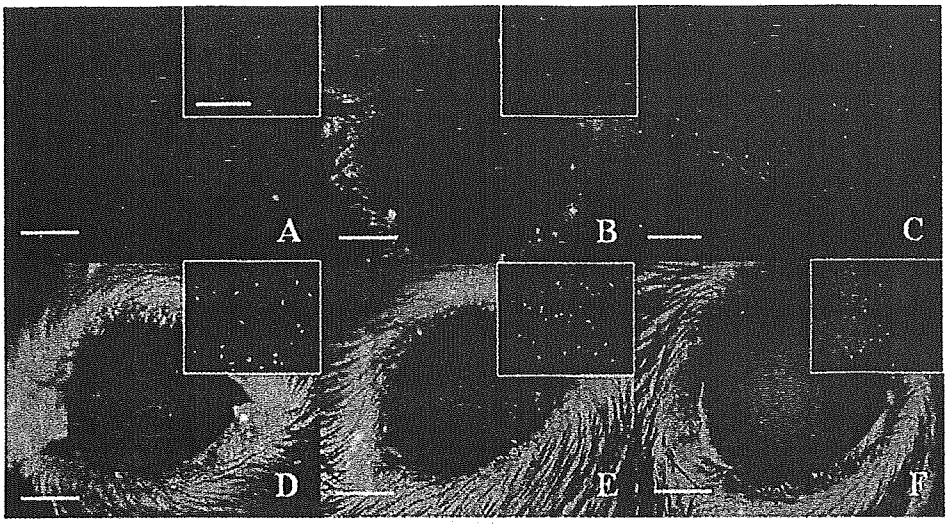

FIGURE 2. Representative time-course slit lamp photographs of murine eyes after BM cell transplantation. (A) One week, (B) 2 weeks, and (C) a high magnification of (B) at the limbal area; (D) 1, (E) 2, and (F) 6 months after transplantation. *Boxes* contain data from the center of the cornea. In the early stages (within the first week) after BM cell transplantation, we observed no GFP^+ cells in the recipient mouse cornea (A). Within 2 weeks, there was intense staining for GFP^+ cells in the periphery of the cornea (B, C). Within 2 months, GFP^+ cells appeared to migrate into the center of the cornea. Their numbers increased in both the periphery and center of the cornea (D, E). Starting at 2 months after BM transplantation, cell density reached a plateau that persisted up to 6 months (F). Scale bars: (A, B, D–F) 1 mm; (C and *insets*) 250 μm.

Cryostat sections (7 μm in thickness) were placed on gelatin-coated slides, air-dried, and rehydrated in PBS at room temperature for 15 minutes. To block nonspecific binding, the tissues were incubated with both anti-Fc receptor mAb (CD16/32; BD PharMingen, San Diego, CA) and 2% bovine serum albumin (BSA) for CD11c and CD11b and with 2% BSA and 10% donkey serum for CD45 at room temperature for 30 minutes. Then the sections were incubated at room temperature for 1 hour with the primary antibody and washed three times in PBS containing 0.15% Triton X-100 (PBST) for 15 minutes. The controls were incubated with the appropriate normal rat and hamster IgG (Dako, Kyoto, Japan) at the same concentration as, but without, the primary antibody. After staining with the primary antibody (CD11c, CD45), the sections were incubated at room temperature for 1 hour with appropriate secondary antibodies, Cy3-conjugated goat anti-hamster IgG, and Cy3-conjugated donkey anti-rat IgG. After several washes with PBS, the sections were coverslipped using antifade mounting medium, with or without propidium iodide (PI; Vectashield; Vector Laboratories) and examined under a confocal microscope (Fluoview; Olympus, Tokyo, Japan).

Quantitative Evaluation

For statistical assessment of corneal cell distribution and characterization, four different fields and six different sections of each cornea were analyzed (24 areas/eye). For analytical purposes, each cornea was divided into central and peripheral areas. The central area was defined as the area within 1 mm of the center and the peripheral area as that within a 1- to 1.5-mm radial distance from the center.

RESULTS

Migration of BM Cells into the Cornea

In the early stages (first week) after BM cell transplantation, there were no GFP^+ cells in the recipient mouse cornea (Fig. 2A). Within 2 weeks of transplantation, some GFP^+ cells appeared in the periphery of the cornea. However, only a small number of GFP^+ cells were present in the center of the cornea (Figs. 2B, 2C). Within 2 months, the number of GFP^+ cells in both the periphery and center of the cornea gradually increased. From 2 months after BM cell transplantation, the cell density reached a relative plateau that persisted up to 6 months (Figs. 2D–F). Our quantitative analysis of GFP^+ cells in the mouse cornea is summarized in Figure 3.

Distribution of BM Cells and HSCs

To determine whether there were BM-derived GFP^+ cells in the recipient cornea, we performed histologic analysis under a dual-channel fluorescence microscope. Cross-sections of recipient corneas showed that most of the GFP^+ cells were distributed in the peripheral corneal stroma and that cell density gradually decreased toward the center (Fig. 4A–D). In the entire corneal epithelium, we noted only a small number of

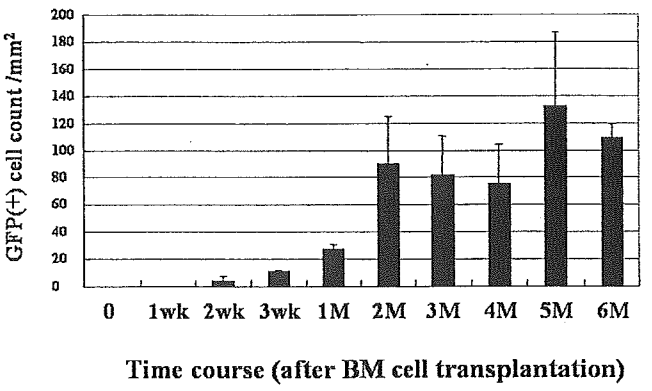

FIGURE 3. Quantitative analysis of GFP^+ cells in the mouse cornea at the indicated times after BM cell transplantation. During the first 2 months, the number of GFP^+ cells gradually increased. Thereafter, cell density reached a relative plateau that persisted up to 6 months after transplantation.

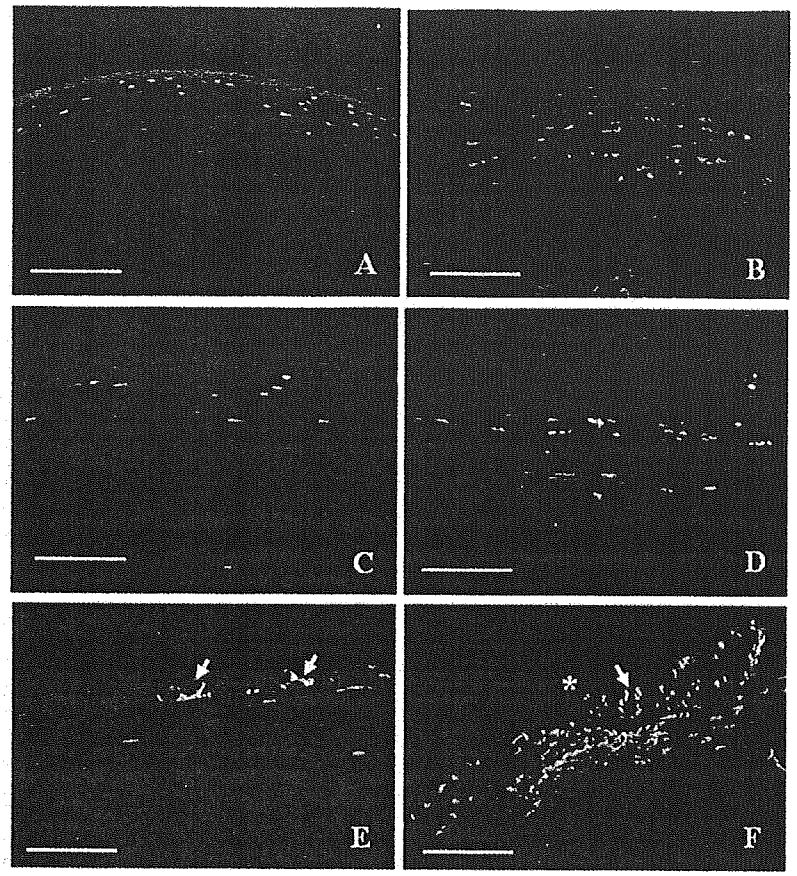

FIGURE 4. Representative cross sections of recipient corneas (A, B, E, BM transplantation; C, D, F, HSC transplantation) show that most of the GFP$^+$ cells were distributed in the peripheral corneal stroma and that the cell density gradually decreases toward the center (A, C, central area; B, D, peripheral area). Only a small number of GFP$^+$ cells were observed throughout the epithelium (E, *arrows*). In contrast, in conjunctival epithelium, several GFP$^+$ cells were noted (F, *arrow*; area to the right of the conjunctiva *). Cell nuclei were stained with PI (*red*). Scale bars: (A, B, F) 200 μm; (C, D, E) 100 μm.

these cells (Fig. 4E), whereas in the conjunctival epithelium we observed several GFP$^+$ cells (Fig. 4F). The percentage of GFP$^+$ cells per section was calculated as the number of GFP$^+$ cells divided by the total number of PI$^+$ cells $\times$ 100. In the peripheral cornea of mice receiving BM cell transplants, GFP$^+$ cells were 2.03% $\pm$ 1.87% (epithelium) and 27.3% $\pm$ 11.1% (stroma). At the center of the cornea, they were 0.93% $\pm$ 0.65% (epithelium) and 7.58% $\pm$ 2.63% (stroma). By contrast, in the peripheral corneas of mice transplanted with HSC, GFP$^+$ cells were 0.78% $\pm$ 0.51% (epithelium) and 24.0% $\pm$ 8.01% (stroma). At the center of the cornea, they were 0.58% $\pm$ 0.4% (epithelium) and 8.06% $\pm$ 1.76% (stroma; Fig. 5). The differences between epithelium and stroma in each category were statistically significant (Mann-Whitney test; $P < 0.01$).

Immunohistochemical Analysis

To characterize BM-derived GFP$^+$ cells in corneal tissue, primarily the corneal stroma, we used fluorescence immunohistology with antibodies to the leukocyte markers CD11c, CD11b, and CD45. Negative control sections, incubated with normal rat and hamster IgG but without the primary antibody, exhibited no discernible specific immunoreactivity over the entire region.

CD11c$^+$ or CD11b$^+$ indicate cells coexpressing GFP and CD11c or GFP and CD11b, respectively. The percentage of CD11c$^+$ or CD11b$^+$ cells was calculated by dividing the respective number of cells by the total number of GFP$^+$ cells $\times$ 100. In the corneal peripheral stroma of BM cell recipients, we observed 19.4% $\pm$ 9.93% CD11c$^+$ cells and 38.7% $\pm$ 16.3% CD11b$^+$ cells. In the central stroma, 15.3% $\pm$ 8.94% were CD11c$^+$ cells and 48.7% $\pm$ 13.1% were CD11b$^+$ cells. In the corneal peripheral stroma of HSC recipients, there were 35.7% $\pm$ 14.0% CD11c$^+$ cells and 56.7% $\pm$ 22.4% CD11b$^+$ cells. In the central stroma, 41.5% $\pm$ 17.8% were CD11c$^+$ cells and 53.7% $\pm$ 13.9% were CD11b$^+$ cells (Figs. 6 , 7, 8). Most GFP$^+$ cells in the cornea were immunostained with CD45 in both BM- and HSC-recipients (Fig. 9). Asterisks in Figure 8 indicate statistically significant difference between CD11c$^+$ and CD11b$^+$ (Mann-Whitney test; $^*P < 0.01$, $^{**}P < 0.05$).

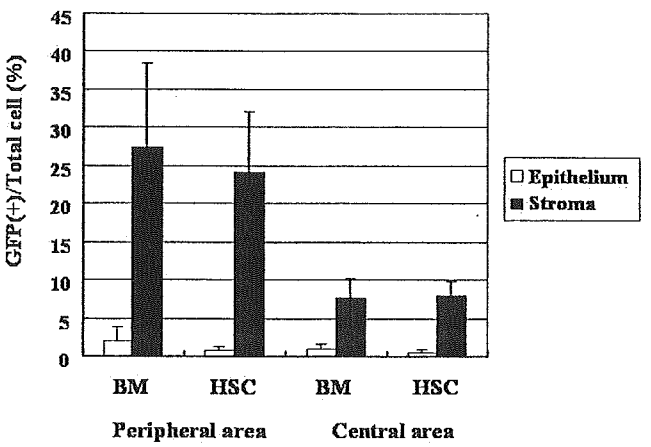

FIGURE 5. Distribution of GFP$^+$ cells in the cornea of mice transplanted with BM cells or HSCs. The percentage of GFP$^+$ cells per section was calculated as the number of GFP$^+$ cells divided by the total number of PI$^+$ cells plus GFP$^+$ cells $\times$ 100. Most of the GFP$^+$ cells were distributed in the peripheral corneal stroma. Cell density gradually decreased toward the center. In the entire area covered by epithelium, there were only a few GFP$^+$ cells. The differences between epithelium and stroma in each category were statistically significant (Mann-Whitney test; $P < 0.01$).

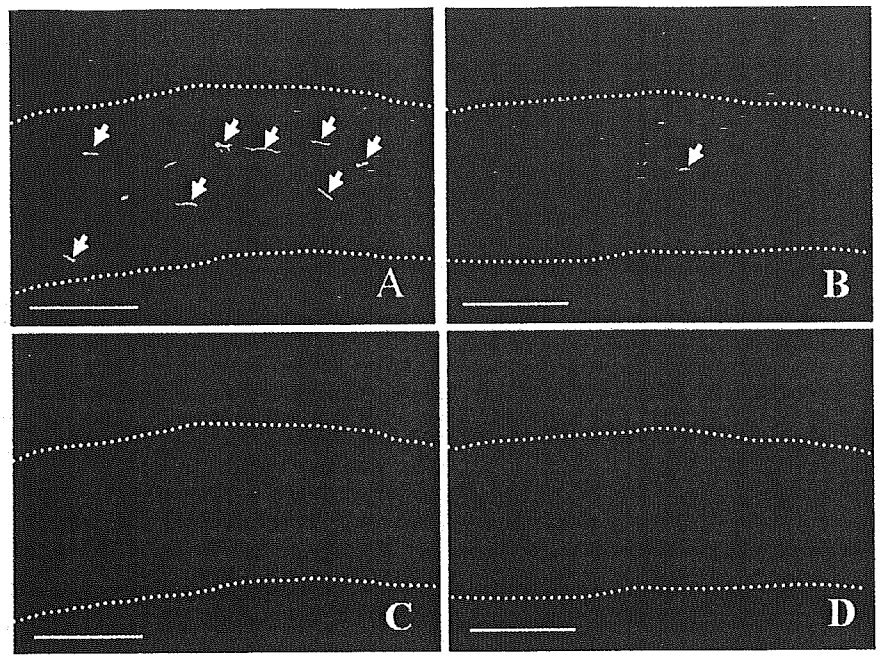

FIGURE 6. Representative immunohistochemical staining for CD11c (*red*) in the peripheral (**A**, **C**) and central (**B**, **D**) cornea of mice receiving HSC transplants. Some GFP^+ cells (*green*) immunostained with CD11c (*arrows*). Note the presence of GFP^+CD11c^- cells throughout the transplant-recipient cornea. GFP (**A**, **B**), CD11c (**C**, **D**). *Dotted lines*: perimeter of whole corneal tissue. Scale bars, 100 μm.

DISCUSSION

The cornea is a transparent, avascular tissue, with integrity maintained by various factors derived from the tear film and aqueous humor. Although the normal cornea does not contain vessels, there is indirect immunohistochemical evidence that it is endowed with a significant number of resident BM-derived APCs.[11–13] Hamrah et al.[11] reported that corneal epithelium contains major histocompatibility complex (MHC) class II-negative Langerhans' cells and corneal stroma a large number of resident BM-derived cells of different lineages. These cells were not only macrophages but also $CD11c^+$ dendritic cells. Brissette-Storkus et al.[12] also documented that the normal murine corneal stroma contains a significant number of $CD45^+$ leukocytes and that most of these cells are monocytes or macrophages. However, to date, there has been no direct demonstration of their existence. BM-derived stem cells, such as hematopoietic- and mesenchymal stem cells, have extensive differentiation capacity.[8,9] We considered two possible mechanisms of BM-derived cell differentiation: One is that BM-derived stem cells that have differentiated into APCs such as Langerhans' cells or macrophages migrate into corneal tissue. Alternatively, BM-derived stem cells transdifferentiate into corneal cells such as corneal keratocytes, and function in the cornea. We examined these possibilities using our unique protocol and found that some BM-derived cells were definitely distributed in the cornea. We also determined that these cells are partially of BM-derived APC lineage, a finding that directly confirms the cell origin of

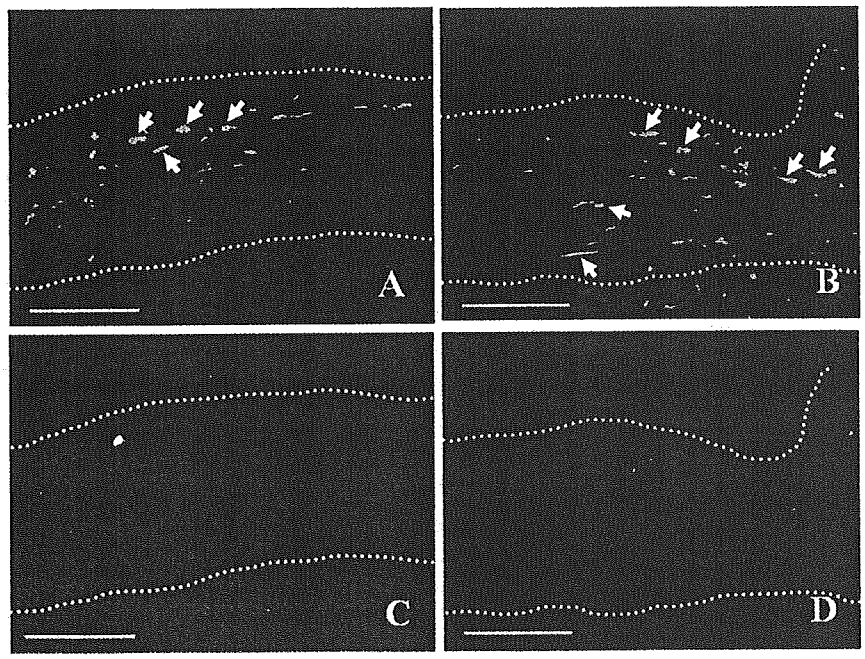

FIGURE 7. Representative immunohistochemical staining for CD11b (*red*) in the cornea of mice receiving BM cell (**A**, **C**) or HSC (**B**, **D**) transplants. Some GFP^+ cells (*green*) immunostained with CD11b (*arrows*). Note the GFP^+CD11b^- cells dispersed throughout the transplant-recipient cornea. GFP (**A**, **B**), CD11b (**C**, **D**). *Dotted lines*: whole corneal tissue. Scale bars, 100 μm.

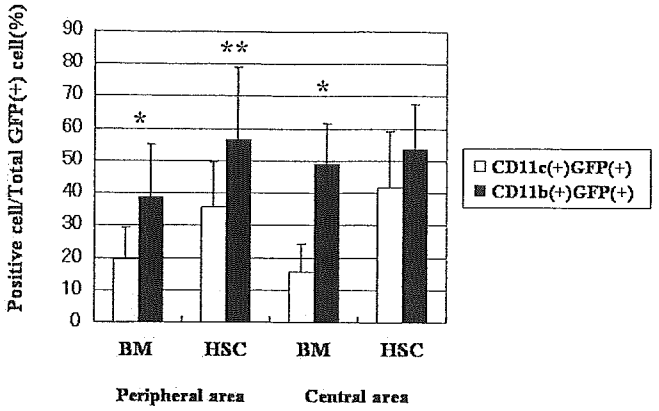

FIGURE 8. Quantitative analysis of the immunohistochemistry for CD11c and CD11b in the cornea of mice receiving transplants of BM cells or HSCs. The percentage of positive cells per section was calculated as the number of cells that coexpressed GFP and CD11c or GFP and CD11b, divided by the total number of GFP^+ cells × 100. The number of $CD11c^+$ cells in both the peripheral and central areas of the cornea was greater in mice receiving transplants of HSCs than in those receiving BM cells. Approximately 50% of GFP^+ cells were immunostained with CD11b in both BM cell and HSC recipients. There were statistically significant differences between $CD11c^+$ and $CD11b^+$ (Mann-Whitney test; $^*P < 0.01$, $^{**}P < 0.05$).

a significant number of resident dendritic cells in the corneal tissue.

Our observations in corneas receiving GFP-labeled BM cell transplants are of particular interest. Ours is the first report on the time course of the migration of GFP-labeled BM cells into the cornea. Within 2 months after BM cell transplantation, the density of GFP-labeled cells gradually increased; thereafter, cell density was comparatively stable, and finally, at 6 months, it reached a plateau. These findings led us to the interesting hypothesis that BM-derived cells continuously migrate into corneal tissue and contribute to corneal integrity. At present, we do not know the longevity of GFP-labeled BM cells in the mouse cornea. Using other experimental protocols, further cell biological study is needed to clarify this point.

There have been no reports on the distribution of hematopoietic stem/progenitor cells (not bone marrow cells) in the mouse cornea. Although the type of transplantation necessary to obtain these data is very difficult, our group has mastered the technique by using a unique protocol that facilitates our long-term observation of the eyes of transplant-recipient mice.

Our study demonstrates that most of the GFP^+ cells were distributed in the corneal stroma: Approximately 25% were found in the periphery and 7% in the center. In contrast, a small number, approximately 1%, were found in the corneal epithelium. The distribution rates of GFP^+ cells were similar in mice receiving with BM cells and HSCs. These results suggest that cells migrating into the corneal tissue may be definite populations of BM cells, such as HSCs or undifferentiated progenitor cells.

Based on our immunohistochemical results, we divided GFP^+ cells in the corneal tissue into four groups: GFP^+CD11c^+, GFP^+CD11b^+, GFP^+CD11c^-, and GFP^+CD11b^- cells. GFP^+CD11c^+ cells (approximately 40% in the HSC transplantation experiment) are thought to express the dendritic cell phenotype[20–22] and GFP^+CD11b^+ cells (approximately 55% in HSCs) either the dendritic cell or macrophage phenotype.[23] Using a protocol similar to ours, Espinosa-Heidmann et al.[24] found that BM-derived progenitor cells contributed to experimental choroidal neovascularization. When they used the F4/80 antibody (monocyte marker), they observed $GFP^+F4/80^+$ cells in the limbus, ciliary body, and normal choroid and sclera, suggesting a high turnover and recruitment rate of infiltrated macrophages. Based on their findings and our observations, we postulate that some of the GFP^+ cells in the mouse cornea are BM-derived APCs.

Some of the GFP^+ cells were negative for cell-surface markers for APCs (CD11c and CD11b), and their origin is unclear. Corneal stroma is composed of both corneal keratocytes and a variety of extracellular matrices comprising collagen subtypes. In our experience, the morphology of GFP^+ cells in the corneal stroma and of corneal keratocytes is very similar. If BM-derived stem cells terminally transdifferentiate into corneal keratocytes, they can be expected eventually to lose surface CD45 expression. We posit that our immunologic experiment did not detect immature $Sca\text{-}1^+$ cells in the mouse cornea (data not shown), suggesting that transplanted hematopoietic stem/progenitor cells first homed to BM and engrafted in the recipient mice, and then provided mature BM-derived cells in the cornea. Based on our present results we cannot unequivocally claim that BM-derived GFP^+ cells can transdifferentiate into corneal cell phenotypes or neurons. Therefore, morphologic and immunohistochemical studies are under way to examine extracellular matrices and cell-surface markers that are uniquely synthesized by corneal keratocytes.

Several technical and conceptual issues deserve consideration in the interpretation of our results. It is important to note that even in eGFP mice significantly fewer than 100% of the cells express GFP. As this may be due to cell-cycle dependent expression of GFP, we suggest that our results underestimate the potential contribution of BM-derived cells in the mouse cornea. We are currently investigating whether the findings we made with our animal model are applicable to humans. Therefore, we are studying the distribution of BM-derived cells in human corneas.

In conclusion, ours is the first study that presents direct evidence for the migration into the cornea of GFP-labeled BM-derived cells. We provide immunohistochemical evidence that some of the migrating cells were BM-derived cells such as

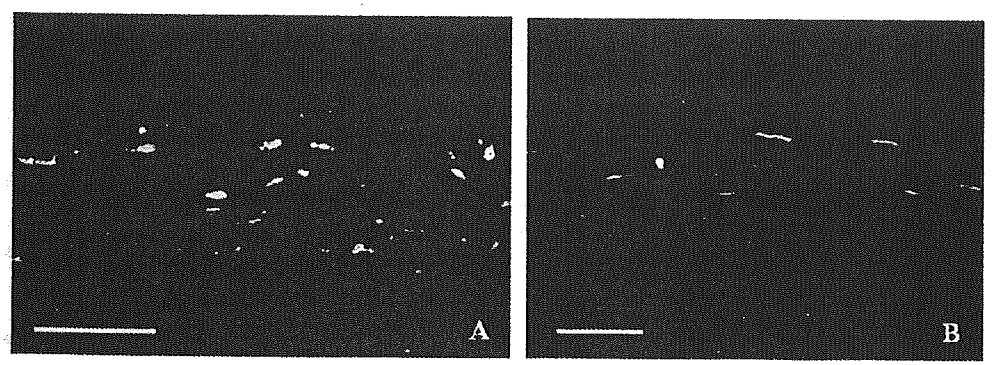

FIGURE 9. Representative immunohistochemical staining for CD45 (*red*) in the cornea of HSC-recipient mice. (A) Peripheral, (B) central retina. Most GFP^+ cells were immunostained with CD45 (*yellow*). Scale bars: (A) 100 μm; (B) 50 μm.

dendritic cells and macrophages. Cell biology studies will determine the lineage(s) of the other cells.

Acknowledgments

The authors thank Hisayo Sogabe for assisting in the immunohistochemical studies and quantitative evaluations.

References

1. Reynolds BA, Weiss S. Generation of neurons and astrocytes from isolated cells of the adult mammalian central nervous system. *Science*. 1992;255:1707–1710.
2. Gage FH. Mammalian neural stem cells. *Science*. 2000;287:1433–1438.
3. Tropepe V, Coles BL, Chiasson BJ, et al. Retinal stem cells in the adult mammalian eye. *Science*. 2000;287:2032–2036.
4. Schermer A, Galvin S, Sun TT. Differentiation-related expression of a major 64K corneal keratin in vivo and in culture suggests limbal location of corneal epithelial stem cells. *J Cell Biol*. 1986;103:49–62.
5. Cotsarelis G, Cheng SZ, Dong G, Sun TT, Lavker RM. Existence of slow cycling limbal epithelial basal cells that can be preferentially stimulated to proliferate: implications on epithelial stem cells. *Cell*. 1989;57:201–209.
6. Prockop DJ. Marrow stromal cells as stem cells for nonhematopoietic tissues. *Science*. 1997;276:71–74.
7. Weissman IL. Translating stem and progenitor cell biology to the clinic: barriers and opportunities. *Science*. 2000;287:1442–1446.
8. Pittenger MF, Mackay AM, Beck SC, et al. Multilineage potential of adult human mesenchymal stem cells. *Science*. 1999;284:143–147.
9. Krause DS, Theise ND, Collector MI, et al. Multi-organ, multilineage engraftment by a single bone marrow-derived stem cell. *Cell*. 2001;105:369–377.
10. Jiang Y, Jahagirdar BN, Reinhardt RL, et al. Pluripotency of mesenchymal stem cells derived from adult marrow. *Nature*. 2002; 418:41–49.
11. Hamrah P, Zhang Q, Liu Y, Dana MR. Novel characterization of MHC class II-negative population of resident corneal Langerhans cell-type dendritic cells. *Invest Ophthalmol Vis Sci*. 2002;43:639–646.
12. Brissette-Storkus CS, Reynolds SM, Lepisto AJ, Hendricks RL. Identification of a novel macrophage population in the normal mouse corneal stroma. *Invest Ophthalmol Vis Sci*. 2002;43:2264–2271.
13. Hamrah P, Liu Y, Zhang Q, Dana MR. The corneal stroma is endowed with a significant number of resident dendritic cells. *Invest Ophthalmol Vis Sci*. 2003;44:581–589.
14. Ishikawa F, Livingston AG, Wingard JR, Nishikawa S, Ogawa M. An assay for long-term engrafting human hematopoietic cells based on newborn NOD/SCID/beta2-microglobulin(null) mice. *Exp Hematol*. 2002;30:488–494.
15. Ishikawa F, Livingston AG, Minamiguchi H, Wingard JR, Ogawa M. Human cord blood long-term engrafting cells are CD34+ CD38−. *Leukemia*. 2003;17:960–964.
16. Hisatomi T, Sakamoto T, Sonoda KH, et al. Clearance of apoptotic photoreceptors: elimination of apoptotic debris into the subretinal space and macrophage-mediated phagocytosis via phosphatidylserine receptor and integrin alphavbeta3. *Am J Pathol*. 2003;162: 1869–1879.
17. Okabe M, Ikawa M, Kominami K, Nakanishi T, Nishimune Y. "Green mice" as a source of ubiquitous green cells. *FEBS Lett*. 1997;407:313–319.
18. Nakamura T, Nishida K, Dota A, et al. Elevated expression of transglutaminase 1 and keratinization-related proteins in conjunctiva in severe ocular surface disease. *Invest Ophthalmol Vis Sci*. 2001;42:549–556.
19. Nakamura T, Nishida K, Dota A, Kinoshita S. Changes in conjunctival clusterin expression in severe ocular surface disease. *Invest Ophthalmol Vis Sci*. 2002;43:1702–1707.
20. Leenen, PJ, Radosevic, K, Voerman, JS, et al. Heterogeneity of mouse spleen dendritic cells: in vivo phagocytic activity, expression of macrophage markers, and subpopulation turnover. *J Immunol*. 1998;160:2166–2173.
21. Vremec, D, Zorbas, M, Scoolay, R, et al. The surface phenotype of dendritic cells purified form the mouse thymus and spleen: investigations of the CD8 expression by a subpopulation of dendritic cells. *J Exp Med*. 1992;176:47–58.
22. Metlay JP, Witmer-Pack MD, Agger R, et al. The distinct leukocyte integrins of mouse spleen dendritic cells as identified with new hamster monoclonal antibodies. *J Exp Med*. 1990;171:1753–1771.
23. Ross GD, Vetvicka V. CR3 (CD11b, CD18): a phagocyte and NK cell membrane receptor with multiple ligand specificities and functions. *Clin Exp Immunol*. 1993;92:181–184.
24. Espinosa-Heidmann DG, Caicedo A, Hernandez EP, Csaky KG, Cousins SW. Bone marrow-derived progenitor cells contribute to experimental choroidal neovascularization. *Invest Ophthalmol Vis Sci*. 2003;44:4914–4919.

Available online at www.sciencedirect.com
SCIENCE DIRECT
ELSEVIER
Experimental Eye Research 82 (2006) 293–299
EXPERIMENTAL EYE RESEARCH
www.elsevier.com/locate/yexer

Expression and tissue distribution of p63 isoforms in human ocular surface epithelia

Satoshi Kawasaki[a,*], Hidetoshi Tanioka[a], Kenta Yamasaki[a], Che J. Connon[b], Shigeru Kinoshita[a]

[a]*Department of Ophthalmology, Kyoto Prefectural University of Medicine, 465, Kajii-cho, Hirokoji-agaru, Kawaramachi-dori, Kamigyo-ku, Kyoto 602-0841, Japan*
[b]*School of Optometry & Vision Sciences, Cardiff University, Cardiff, UK*

Received 19 January 2005; accepted in revised form 1 July 2005
Available online 22 August 2005

Abstract

The functional significance of p63 in regulating cell proliferation in various stratified epithelial cells has previously been proposed. More than six isoforms have been reported for this protein; however, it is not yet clearly understood how functionally different these isoforms are. To investigate how these isoforms are used in ocular surface epithelia, we studied the spatial distribution of p63 isoforms within human ocular surface epithelia. Individual layers (basal, intermediate, and superficial) of the human ocular surface epithelia (cornea, limbus, and conjunctiva) were selectively obtained using a laser micro-dissection device. These samples were equally amplified and subjected to RT-PCR analysis with primer pairs, which specifically amplify each of five isoform-determining regions or each of six p63 isoforms. Regarding the N-terminal region, the TA domain was not detected in all samples, while a ΔNp63 specific region was detected in the basal–intermediate region of all types of epithelia and in the superficial layer of the limbus. Regarding the C-terminal region, an α-isoform specific region was detected in all layers of the conjunctiva and limbus, as well as in the basal to intermediate layers of the cornea. A β-isoform specific region was detected in the basal to intermediate layers of the limbus. A γ-isoform specific region was detected in almost all layers of all epithelia. Among the six p63 isoforms, only ΔNp63α was detected in the basal to intermediate layers of the limbus and conjunctiva. These results suggest that ΔNp63α is the most dominant isoform within human ocular surface epithelia. This isoform may contribute, at least in part, to the maintenance of cell proliferative capacity within the ocular surface epithelia.

Keywords: p63; ΔNp63α; alternatively spliced variant; ocular surface epithelia; cell proliferation; laser micro-dissection; RT-PCR

1. Introduction

p63 was first cloned from a rat circumvallate taste papilla cDNA library as a highly homologous gene to p53 (Schmale and Bamberger, 1997), a key player in anti-cancer systems. However, in spite of the significant sequence similarity between these two proteins, p63 is not used in tumour suppression, but in development. The function of p63 was elegantly shown using knockout (KO) mice, in which the absence of p63 results in severe anomalies in limb and craniofacial morphogenesis, as well as severe hypoplasia of squamous epithelia (Mills et al., 1999; Yang et al., 1999).

From these previous studies, a significant role of p63 in maintaining squamous epithelia has been presumed. Yang et al. (1999) proposed a model in which p63 may help epithelial stem cells retain their proliferative capacity. Later, Pellegrini et al. (2001) reported the expression of p63 in young transient amplifying (TA) cells and stem cells of the epidermal and corneal epithelia, proposing that this protein is a specific marker for keratinocyte stem cells. Since then, p63 has been used as a putative stem-cell marker in limbal and cultivated corneal epithelial cells (Harkin et al., 2004).

More than six isoforms have been reported for the p63 protein (Yang et al., 1998). The N-terminus region exhibits two alternative transcription initiation sites, giving rise to two different N-termini, including the TA isotype, which

* Corresponding author. Satoshi Kawasaki, Department of Ophthalmology, Kyoto Prefectural University of Medicine, 465, Kajii-cho, Hirokoji-agaru, Kawaramachi-dori, Kamigyo-ku, Kyoto 602-0841, Japan.
E-mail address: skawasak@eye.ophth.kpu-m.ac.jp (S. Kawasaki).

0014-4835/$ - see front matter © 2005 Elsevier Ltd. All rights reserved.
doi:10.1016/j.exer.2005.07.001

contains/is the *trans*-activating domain, and the ΔNp isotype, which lacks this domain. The C-terminus region exhibits three alternative splicing patterns, giving rise to three types of C-termini, including α, β, and γ isotypes. The combination of the two N-termini and three C-termini produces a total of six isoforms for the p63 protein. In addition, special types of p63, designated as TA*p63 (Yang et al., 1998), which has an additional 39 amino acids in the N-terminus, and ΔNp73L, which corresponds to ΔNp63 lacking exon 4, have also been discovered (Foschini et al., 2004).

Precise analysis of p63 expression within ocular surface epithelia, including detailed information regarding these isoforms, will contribute to understanding how this protein is used in the maintenance of ocular surface epithelia. At present, several antibodies raised against different portions of p63 isoforms are commercially available. However, as described above, regions that determine each specific p63 isoform are located separately at the N-terminus and C-terminus, making it unlikely that a single antibody is able to detect a specific type of p63 isoform. Therefore, using pairs of PCR primers to distinguish the individual p63 isoforms, we investigated the expression of individual p63 isoforms by RT-PCR analysis against the individual layers of human ocular surface epithelia. We found that ΔNp63α is the most dominant type of p63 isoform within human ocular surface epithelia and that this isoform is specifically located within the basal to intermediate layers of the limbal and conjunctival epithelia.

2. Materials and methods

2.1. Human subjects

This research was conducted after a thorough review and approval by the Committee for Ethical Issues on Human Research of Kyoto Prefectural University of Medicine and in accordance with the tenets of the Declaration of Helsinki. Permission to use corneas for research was obtained from all of the families of the deceased.

Three human corneo-scleral tissues were obtained from three donors (a 79-year-old male and two 54-year-old females) approximately 6 hr after death at the North–West Lion Eyebank (Seattle, WA, USA). Each donor was free of any ocular surface disorder or history of eye surgery. Before embedding, the surface conditions of each of the corneo-scleral tissues were inspected using a binocular slit lamp and were found to be free of apparent epithelial damage.

2.2. RT-PCR analysis for laser micro-dissected samples

The three corneo-scleral tissues were snap-frozen in Tissue-Tek® OCT compound (Sakura Finetechnical, Tokyo, Japan) with liquid nitrogen. Corneo-scleral sections of 10 μm were cut and placed onto either a silanated or a specialized glass-slide (Penfoil slide; Leica Microsystems, Tokyo, Japan) for immunostaining or laser micro-dissection, respectively. Individual epithelial layers (basal, intermediate, superficial) from the three ocular surface epithelia were dissected using a laser micro-dissection device (AS LMD; Leica Microsystems, Wetzlar, Germany). Keratin 12 is known as a corneal epithelial specific keratin (Kurpakus et al., 1990, 1994) and is thought not to be expressed in limbal basal stem cells. Therefore, only cells negative for keratin 12 were collected for the limbal basal cell samples using the laser micro-dissection device (Fig. 1). This process was achieved by viewing serial adjacent sections that were immunostained with keratin 12. Total RNA was extracted from each of the laser micro-dissected samples with TRIZOL reagent (Invitrogen, Carlsbad, CA, USA) according to the manufacturer's guidelines. The RNAs were reverse-transcribed and amplified using a Super SMART PCR cDNA synthesis kit (BD Bioscience, Tokyo, Japan) according to the manufacturer's guidelines. Briefly, cDNAs were synthesized from the extracted RNAs using 0.84 μM 3′ SMART CDS Primer IIA [AAGCAGTGGTATCAACGCAGAGTACT(30)VN; V= A or C or G] and 0.84 μM SMART IIA oligonucleotide (AAGCAGTGGTATCAACGCAGAGTACGCGGG) in a buffer containing 1× first-strand buffer, 2 mM dithiothreitol (DTT), 0.2 mM dNTP, 1 U/μl RNase inhibitor and 1/20 volume of PowerScript reverse transcriptase. After purification using standard column chromatography, the cDNAs were amplified by PCR with 0.24 μM 5′ PCR Primer IIA (AAGCAGTGGTATCAACGCAGAGT) in 100 μl of reaction buffer containing 1× Advantage 2 PCR buffer, 0.2 mM dNTP and 1× Advantage 2 polymerase mix. The thermal conditions used were an initial denaturation step (95°C for 1 min), followed by an amplification cycle (95°C for 5 sec, 65°C for 5 sec, and 68°C for 3 min). The cycle number was optimized for each sample as follows. First, each sample was amplified with 15 cycles using the above thermal conditions. Then the thermal cycling was paused and a 10-μl aliquot was removed from each sample and stored at 4°C before the following optimization process was completed. Next, the thermal cycle was resumed and a 5-μl aliquot was removed from each sample after cumulative cycle numbers 18, 21, 24, 27, 30, and 33. All aliquots from all samples were electrophoresed in 2% agarose gel to estimate the number of cycles required to reach the plateau phase of amplification for each sample. The optimized cycle number was determined as one cycle fewer than that needed to reach the plateau. Then each stored sample was amplified again up to the individual optimized cycle number. The PCR products were electrophoresed in 2% agarose gel to assure the cDNA amplification and to estimate their amounts. The amplified cDNA samples were diluted to normalize their

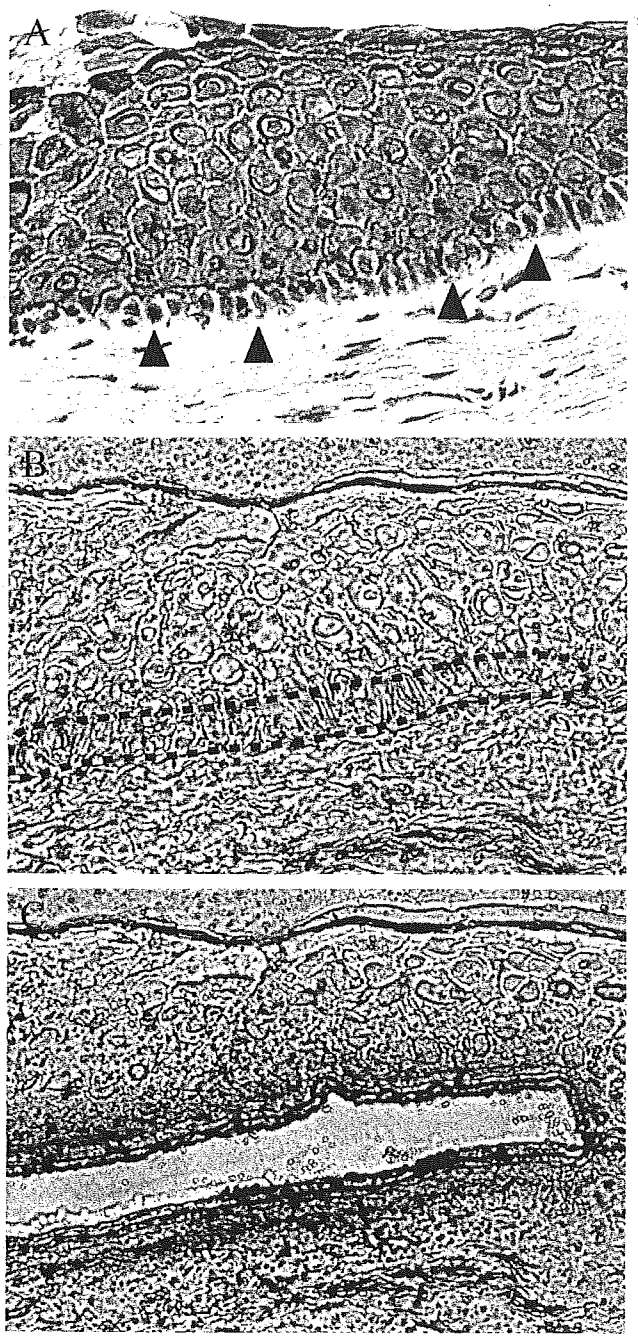

Fig. 1. Laser micro-dissection of the limbal basal layer. Corneo-scleral tissue was immunostained with an anti-keratin 12 antibody (sc-17098, Santa Cruz Biotechnology) using a standard indirect immunostaining procedure and developed with DAB (brown). Counter-staining was performed with hematoxylin. Limbal basal cells, which contain putative stem cells, are negative for keratin 12 (A, arrowhead). (B) Unstained section contiguous to A. The red dotted line denotes limbal basal cells, which are negative for keratin 12, as shown in A. (C) Same section as B after laser micro-dissection. The dissected area is somewhat larger than the red dotted area because of the width of the laser cutting line.

concentrations according to their electrophoresis intensity. Expression of p63 isoforms was examined by RT-PCR with isoform-specific primer pairs (Table 1) using the amplified cDNAs as PCR templates. The PCR products were electrophoresed in 1 or 2% agarose gel and stained with ethidium bromide.

2.3. Cloning of the six p63 isoforms and validation of the six p63 isoform-specific primer pairs

Skin RNA (Stratagene, La Jolla, CA, USA) was reverse-transcribed using a random hexamer primer (Invitrogen). The six p63 isoforms were amplified by PCR with the corresponding specific primers using this cDNA. After checking by electrophoresis, the PCR products were ligated to a TA cloning vector (pGEM-T easy vector; Promega, Madison, WI, USA) followed by transformation to chemically competent cells (JM 109; TOYOBO, Tokyo, Japan). After checking by sequencing analysis, each clone containing an individual wild-type p63 isoform was cultured, harvested and subjected to plasmid extraction using a standard column-based procedure. TAp63β and TAp63γ, which were not amplified by above RT-PCR, were obtained by connecting independently amplified fragments of the TAp63 common region and the β or γ region, respectively. Using these plasmids, the six primer pairs were checked to determine whether or not they were functional.

2.4. Immunostaining

The sections were fixed with Zamboni's fixative at 4°C for 5 min. After washing, the sections were incubated in a blocking buffer containing 0.01 M phosphate-buffered saline (PBS) and 1% bovine serum albumin (BSA) at room temperature for 30 min. The sections were then incubated with an anti-keratin 12 antibody (sc-17098, ×100, Santa Cruz Biotechnology, Santa Cruz, CA, USA) or normal goat IgG (×100, Santa Cruz Biotechnology) at 4°C overnight. After another wash, the sections were incubated with a secondary antibody solution (biotin-labelled anti-goat IgG, Invitrogen) at room temperature for 1 hr. The sections were washed again and incubated with a horseradish peroxidase (HRP)-labelled streptavidin solution (×100, Amersham Biosciences) at room temperature for 1 hr. After a final wash, the sections were developed with diaminobenzidine (DAB; Dojindo, Kumamoto, Japan) followed by counter-staining with hematoxylin.

2.5. Southern blot analysis

Amplicons were validated by Southern hybridization using biotin-labelled oligoprobes franked by the corresponding primer pairs (ΔNp domain, CAGATTCA-GAACGGCTCCTC; α specific region, ATCGCATGTC-GAAATTGCTC; αβ sharing region, GTCTCACT GGAGCCCACACT; γ specific region, GGGGGCTT GGAATGTCTAAA; ΔNp63α, TGGAGAGAGAGCATC-GAA GG; keratin 12, TGAATGGTGAGGTGGTCTCA; β-actin, AAGTACTCCGTGTGGATCGG). Biotinylated